energies

MDPI

Article

Design and Analysis of a Hybrid Stand-Alone Microgrid

Muhammad Zubair Asif Bhatti [1], Abubakar Siddique [1], Waseem Aslam [2,*] and Shahid Atiq [1]

[1] Department of Electrical & Biomedical Engineering, Khwaja Fareed University of Engineering and Information Technology (KFUEIT), Rahim Yar Khan 64200, Pakistan; zubairasif02@gmail.com (M.Z.A.B.); dr.abubakar@kfueit.edu.pk (A.S.); shahid.atiq@kfueit.edu.pk (S.A.)

[2] Department of Electrical, Electronics and Computer Systems, University of Sargodha (UOS), Sargodha 40100, Pakistan

* Correspondence: wasimevergreen@yahoo.com

Abstract: This research article presents a comprehensive investigation into the design, optimization, and performance analysis of a hybrid stand-alone microgrid for an industrial facility in Iraq at coordinates 36.51 and 43.99. The system consists of photovoltaic (PV) modules, inverters, a battery energy storage system (BESS), a generator, and AC loads. Leveraging the capabilities of PVsyst version 7.3.1, HOMER Pro version 3.14.2 and SAM version 2022.11.21 software tools, this study assesses the feasibility and functionality of the hybrid stand-alone microgrid. In this study, PVsyst software is used for detailed designing and analysis of a PV plant, and the PVsyst design file is then used in HOMER Pro software to optimize and design the proposed hybrid stand-alone microgrid, and for detailed performance analysis SAM software is employed. This paper also investigates the impact of ground clearance and ground albedo on the annual generation of bifacial PV modules at various tilt angles. Key findings include a promising normalized production rate of 4.53 kWh/kWp/day with a performance ratio of 0.815 and annual energy production estimates of 84.31 MWh (P50), 79.57 MWh (P90), and 78.24 MWh (P95) for monofacial PV modules, highlighting the system's potential for renewable energy generation. Notably, this research demonstrates the hybrid stand-alone microgrid's capacity to significantly reduce CO_2 emissions, saving approximately 1811.6 tons over a 30-year period, thus contributing to sustainability and environmental conservation goals. Additionally, this study reveals operational challenges during the winter months, necessitating generator support to meet load demands. The successful installation and experimental validation of the hybrid stand-alone microgrid underscore its practical viability and its role in advancing clean energy solutions. This research provides valuable insights into hybrid stand-alone microgrid design, emphasizing its importance in ensuring reliable power supply and environmental stewardship.

Keywords: distributed generation (DG); energy storage system (ESS); photovoltaic (PV); battery energy storage system (BESS); electrical diesel generator (EDG); Hybrid Optimization Model for Electric Renewables (HOMER); performance ratio (PR); renewable energy sources (RES); system advisor model (SAM)

Citation: Bhatti, M.Z.A.; Siddique, A.; Aslam, W.; Atiq, S. Design and Analysis of a Hybrid Stand-Alone Microgrid. *Energies* **2024**, *17*, 200. https://doi.org/10.3390/en17010200

Academic Editors: José Matas, Pedro S. Moura and Ana Soares

Received: 9 November 2023
Revised: 24 November 2023
Accepted: 22 December 2023
Published: 29 December 2023

1. Introduction

The conventional means of electrical energy generation, primarily relying on fossil fuel power plants, have long been associated with significant environmental and economic challenges. These drawbacks include detrimental contributions to air pollution and greenhouse gas emissions, leading to climate change and adverse effects on human health. Moreover, such energy production methods are fundamentally unsustainable as they rely on finite resources like coal, oil, and gas, which are inexorably depleting [1,2]. Additionally, these conventional power plants often impose severe consequences on local ecosystems and wildlife through habitat destruction and water pollution. The economic burden of electricity generation through these means is equally substantial, encompassing both financial and environmental costs [3].

Conversely, renewable energy generation has emerged as a promising alternative [4]. However, it is not without limitations. Renewable sources, such as solar and wind power, can be intermittent and subject to the unpredictability of weather conditions [5,6]. This intermittency necessitates the development of backup systems and energy storage solutions [7]. Furthermore, while renewable energy infrastructure costs have decreased over time, the initial investment remains relatively high. Additionally, not all geographical locations are conducive to certain types of renewable energy generation, limiting their widespread adoption [8].

In response to these challenges, microgrids (MGs) have emerged as a viable solution for localized energy generation [9]. These MGs typically comprise components such as low-voltage (LV) distribution systems, distributed energy resources (DERs) (e.g., photovoltaics, fuel cells, micro-turbines), energy storage components (batteries, energy capacitors, and flywheels), and flexible loads [10]. MGs can operate in both non-autonomous (grid-tied) and autonomous (grid-independent) modes, offering flexibility and resilience [11,12].

The HOMER Pro microgrid software from HOMER Energy stands out as the industry standard for microgrid design optimization. It leverages the Hybrid Optimization Model for Multiple Energy Resources (HOMER) to simulate and analyze various equipment configurations to find optimal system designs. HOMER simulates the operation of hybrid microgrids over the course of a year, providing insights at varying time steps, from one minute to one hour [13]. In [14], the focus is on the design, performance analysis, and optimization of a grid-connected hybrid microgrid for hospital applications employing HOMER software. Ref. [15] explores the design of an off-grid (stand-alone) hybrid (AC/DC) microgrid intended for a community system using HOMER software. Ref. [16] presents the optimization of a grid-connected microgrid for three different cities in Pakistan employing HOMER software. In [17], researchers present the modeling and optimization of a community microgrid situated in a housing estate in Cape Town, South Africa, employing HOMER software. Ref. [18] addresses the design considerations for a microgrid in Rwanda, specifically engineered to provide low-cost electricity employing HOMER software. PVsyst software is the best approach for analyzing PV generation, as solar design depends on various factors, including its longitude, range, climatic conditions like temperature, wind speed, and sun-oriented irradiance. By evaluating these factors, it will be possible to increase the efficiency of a sunlight-based PV module and predict the cost of the system [19–23]. Ref. [19] conducts a performance analysis on a grid-connected PV plant generating 4908 MWh annually for a university in Bahawalpur, Pakistan, employing PVsyst software. Ref. [20] focuses on the design and installation of a stand-alone solar PV system, utilizing PVsyst software to meet the annual energy requirement of 1086.24 kWh for a college in India. Ref. [21] details the design of a 100 MW grid-connected PV plant for a university in Saudi Arabia, employing PVsyst software. Ref. [22] delves into the analysis and design of a 700 KWp grid-connected solar power plant in the Daikundi province of Afghanistan using PVsyst software. Ref. [23] presents the modeling and simulation of a 1 MW PV plant in the north of Morocco, employing PVsyst software. SAM software can be used for performance analysis of hybrid microgrids by monitoring and analyzing the software components that contribute to the overall performance of the system [24–30]. Ref. [24] introduces Cascade Extended Analysis as a methodology to ascertain the optimal capacities and sizes of diverse power generation and energy storage systems (ESSs) with a renewable energy plant, applicable to both grid-connected and stand-alone setups, facilitated by SAM software. Ref. [25] conducts an analysis of energy generation from on-grid PV plants across all regions of Brazil. Ref. [29] details the design and performance analysis of an 8 kW PV grid-connected system incorporating an ESS, employing SAM software. Ref. [30] presents an analysis of a PV system and BESS for the community using SAM software.

This research paper is dedicated to the optimization, simulation, performance analysis, and design of hybrid stand-alone microgrids tailored to meet the energy needs of facilities. It aims to validate the proposed designs through empirical test results and experiment

reports. To achieve this, a combination of various software tools will be utilized, each offering distinct advantages and limitations. For instance, PVsyst is particularly valuable for PV plant design and conducting detailed analysis with real-time parameters. HOMER Pro excels in optimization and analysis, while SAM software proves advantageous for studying the performance analysis of hybrid stand-alone microgrids with battery energy storage systems. Including test findings and experiment reports will provide robust validation for the proposed hybrid stand-alone microgrid designs, advancing the field of sustainable energy solutions.

The following is how this paper is structured: In Section 2, a comprehensive overview of the proposed hybrid stand-alone microgrid is presented. It begins with an exploration of the microgrid's structural design, followed by an in-depth analysis of the electrical load schedule and system sizing calculations. The modeling of the photovoltaic (PV) system is then elucidated, covering the design parameters and calculations that are discretized for utilization in PVsyst software, employed in the subsequent PV plant designing phase. Subsequently, the microgrid's design is explicated using HOMER Pro software, incorporating data files from PVsyst software. The section culminates with the performance analysis methodology for the proposed microgrid, employing the System Advisor Model (SAM) software. In the subsequent Section 3, the focus is on the outcomes derived from PVsyst software. This includes an exploration of the impact of ground clearance and ground albedo on the annual generation, considering various tilt angles of bifacial PV modules. For monofacial PV modules integrated into the proposed microgrid, the discussion encompasses daily output energy, normalized production per installed kWp, loss analysis, probability distribution, performance ratio, capacity factor, and saved CO_2 emissions projected over the next 30 years. The results obtained from HOMER Pro software, detailing power injection from the PV system and an emergency diesel generator (EDG) into the microgrid, as well as the expected PV and EDG output power for the entire year, are thoroughly examined. The performance analysis of the microgrid, using SAM software, is then discussed. Finally, the section concludes with an analysis of practical results. This paper concludes with a final section summarizing the key findings and insights gained from this research.

2. Materials and Methods

This section aims to provide a comprehensive understanding of the proposed hybrid stand-alone microgrid. Firstly, it will delve into the structure of the microgrid, highlighting its various components and their interconnections. Following this, the electrical load schedule and system sizing calculation will be discussed, providing insights into the planning and optimization of the microgrid's energy usage. Subsequently, the modeling of the photovoltaic (PV) system will be explained, shedding light on the technical aspects of integrating renewable energy sources into the microgrid. Moving forward, the design of the hybrid stand-alone microgrid will be elaborated upon, emphasizing the considerations and strategies employed. Lastly, the performance analysis of the microgrid will be presented.

2.1. Structure of the Proposed Hybrid Stand-Alone Microgrid

The hybrid stand-alone microgrid taken into consideration in this study will be used to meet the demand requirements of a facility in Iraq. Since there is currently no distribution network in the area where the facility is located, building a dedicated line to the site would need a substantial capital investment. This is the rationale for choosing to build a microgrid. Therefore, an autonomous microgrid would be better from that point of view because energy consumption would then be provided for free during the project's lifespan. Additionally, a microgrid that mainly uses renewable energy sources would make it easier to reduce CO_2 emissions, which would improve the environment and play a significant role in the transition to a carbon-free world.

Photovoltaic (PV) panels, a battery energy storage system (BESS), and a diesel generator form the autonomous system under consideration, which is designed to handle extended periods of darkness, illustrated in Figure 1.

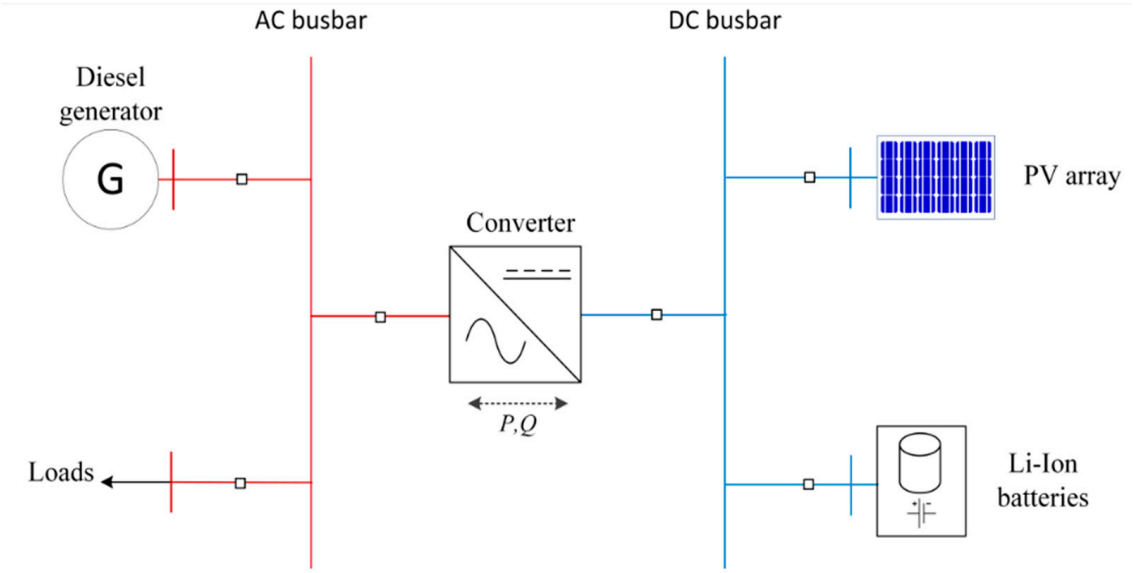

Figure 1. Schematic of hybrid microgrid.

2.2. Electrical Load Schedule and System Sizing Calculation

The site consists of industrial loads. Therefore, the site's peak load will not differ considerably neither during summer and winter nor during weekends and weekdays. The detailed electrical load schedule of an existing facility is presented in Table 1. Note that Table 1 lists the current facility's detailed electrical load schedule, Table 2 lists the input data, and Table 3 lists the sizing calculation of the diesel generator. However, a 50 kVA generator is selected considering the load of the facility as well as the charging load of BESS during an emergency condition. Moreover, Table 4 lists the sizing calculation of BESS.

Table 1. Detailed electrical load schedule.

S.no	Load Description	Total Wattage (W)	hr./day	Amp. hr./day	Watt hr./day
1	Pump Motors	1000	24	60	24,000
2	Control Panel Loads	1040.38	24	109	24,969.12
3	Heat Tracing	500	24	52	12,000
4	Access Control Cabin Loads	3305.5	24	345	79,332
5	Elec. Equipment Room Loads	1700	24	181	40,800
	Total Load in Watts			7546	Watts
	Total Load in Watts with 15% Margin			8678	Watts
	Total Load in Watt hr./day			181,101	W-hr./day
	Total Load in Watt hr./day with 15% Margin			208,266	W-hr./day

Table 2. Input data.

S.no	Description	Value	Unit
1	Three-Phase Voltage	400	V
2	Single-Phase Voltage	220	V
3	Power Factor	0.8	
4	Efficiency	0.9	
5	Largest Motor	0.55	kW

Table 3. Diesel generator sizing.

Calculation of Required Generator Rating under Running Condition		
Total running load in kW	7.5	kW
Total running load in kVAR = kW × Tan($\cos^{-1}(\theta)$)	5.7	kVAR
Total running load in kVA = Sqrt($(kW)^2$ + $(KVAR)^2$)	9.43	kVA
Total running load in KVA with 15% margin	10.85	kVA
Calculation based on largest motor load		
Largest motor load	0.55	kW
Starting current	6	Times
Full load current for largest motor	3.32	Amp
Motor rating (kW/power factor)	0.69	kVA
Motor rating considering the starting current (6 × 0.69)	4.13	kVA
Total running load of the site with largest motor starting current		
Total running load of the plant with 15% margin	10.85	kVA
Largest motor kVA considering the starting current	4.13	kVA
Total kVA required for generator	14.97	kVA

Table 4. BESS sizing.

BESS Sizing Calculation Basis		
Total load (during power supply from battery)	7546	W-hr.
Total load in VA (with the power factor of 0.8)	9432	VA
Battery aging factor (Ag)	0.2	
Battery depth of discharge (DOD)	0.8	
Battery efficiency (η)	0.95	
Total load of BESS in AH		
Backup capacity	16	hr.
BESS voltage	48	V
Total load of BESS = (total load in kW x backup capacity)/battery bank volt	2457	A-hr.
Size of the BESS		
Size of the BESS = [(load in A-hr.) × (1 + Ag)]/[η × DOD]	3200	A-hr.
Number of batteries required		
Selected battery A-hr.	200	A-hr.
Selected battery V	48	V
Total Number of batteries required	16	No.

System sizing is modeled considering the industrial load as essential load. For reliability of power supply, all system components are designed with the torque load of the facility taken into account. Furthermore, the system is designed in such a way that during the sun hours, the PV plant will supply electricity to the load and the BESS, while during off sun hours, the BESS will supply electricity to the load, and a backup diesel generator will supply electricity to the load in an emergency.

2.3. Modeling of PV System

PVsyst version 7.3.1 software is used to model PV systems. PVsyst software is a powerful tool for solar energy system design, simulation, and performance analysis. It allows us to accurately assess the energy production potential of a photovoltaic system by considering factors such as location, shading, module characteristics, and system configuration. With PVsyst, one can optimize system sizing, evaluate different design scenarios, and estimate the financial viability of solar projects. It is a valuable software in the renewable energy industry. Figure 2 illustrates the flowchart for PVsyst software.

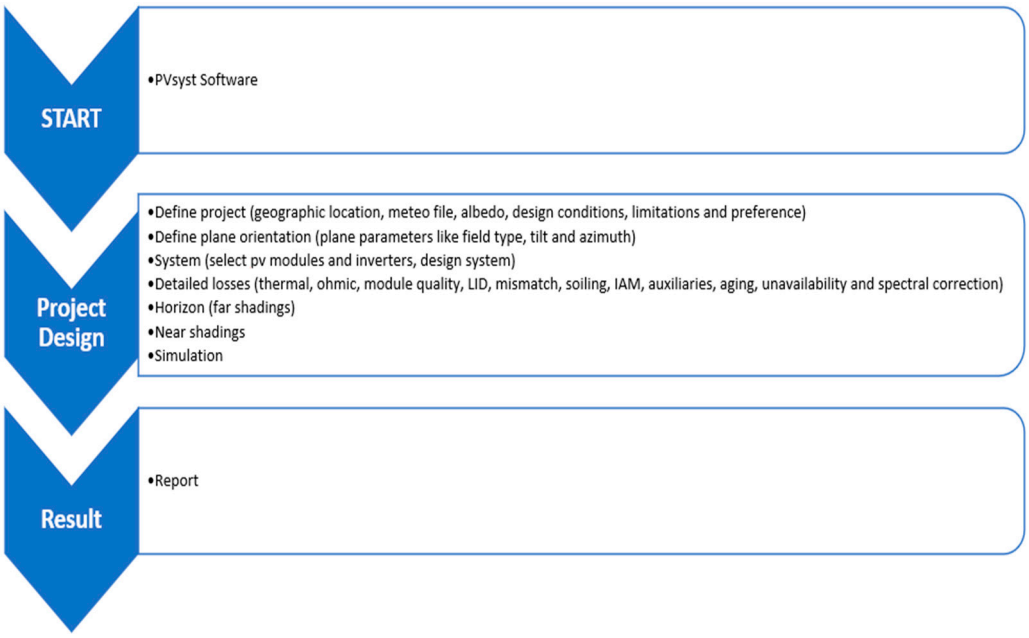

Figure 2. Flowchart for PVsyst software.

Results are presented by PVsyst software as a comprehensive report with relevant graphs and tables. The information may be exported for use in other applications.

PVsyst software is a comprehensive tool used for designing PV arrays with three different methods: grid-connected, stand-alone, and pumping. In this research, the grid-connected method has been selected to design the PV arrays. There are a total of four PV arrays in this design. Three of these arrays consist of one string inverter per PV array and two strings of 13 PV modules per PV array, each module with a power output of 500 Wp. The remaining PV array consists of one string inverter and two strings of 12 PV modules, each with a power output of 500 Wp. These PV arrays are designed for a fixed tilted plane field type arrangement, ensuring optimal sunlight exposure and energy generation during winter.

2.3.1. Define Project

The geographical coordinates of the facility are 36.5144907 and 43.9887378, respectively. The facility is situated in a region of dry mountains. Hence, 0.2 is chosen as the albedo value. Based on data gathered from the site, the following design parameters were taken into consideration for the project: -1 °C for lower temperature for absolute voltage limit, 20 °C for winter operating temperature for VmppMax design, 45 °C for usual operating temperature under 1000 W/m^2, and 50 °C for summer operating temperature for VmppMax design.

$$Irradiance\ of\ location = \frac{Average\ Ins.}{Average\ Sun} \tag{1}$$

Here, Average Sun is the average number of hours per day with bright sunshine, and Average Ins. is the average insolation of the location. The area unit is kWh/m^2.

$$Solar\ Irradiance\left(\frac{W}{m^2}\right) = irradiance(kWh) \times \frac{1000}{hours} \tag{2}$$

The solar radiation data were obtained from Meteonorm version 8.1 and the global solar radiation on horizontal surfaces in the project site, and it was observed that it varies from 234.3 kWh/m^2/month to 77.4 kWh/m^2/month during the complete year. The relatively low observed solar radiation from November to February is due to the prevailing high

moisture content and heavy clouds during the rainy season in this area. The meteorological data of the site are given in Table 5. Additionally, the SOLARGIS in Figure 3 provides a location map of the solar resources.

Table 5. Meteorological data of the site.

Month	Global Horizontal Irradiation kWhr./m^2/mth	Horizontal Diffuse Irradiation kWhr./m^2/mth	Temperature °C	Wind Velocity m/s	Relative Humidity %
January	79.5	34.7	7.3	3.39	64.5
February	92.6	39.5	8.9	3.40	62.9
March	133.0	62.9	13.1	3.60	56.0
April	173.1	72.8	17.2	3.40	53.8
May	198.2	90.3	24.0	3.40	37.4
June	234.3	71.2	30.6	3.80	22.9
July	233.3	71.6	34.7	3.49	20.1
August	214.0	62.6	33.8	3.20	21.8
September	181.2	39.3	28.6	3.19	25.1
October	130.8	44.9	22.7	3.01	35.0
November	92.2	29.5	14.0	3.00	48.7
December	77.4	26.0	9.2	3.30	60.8

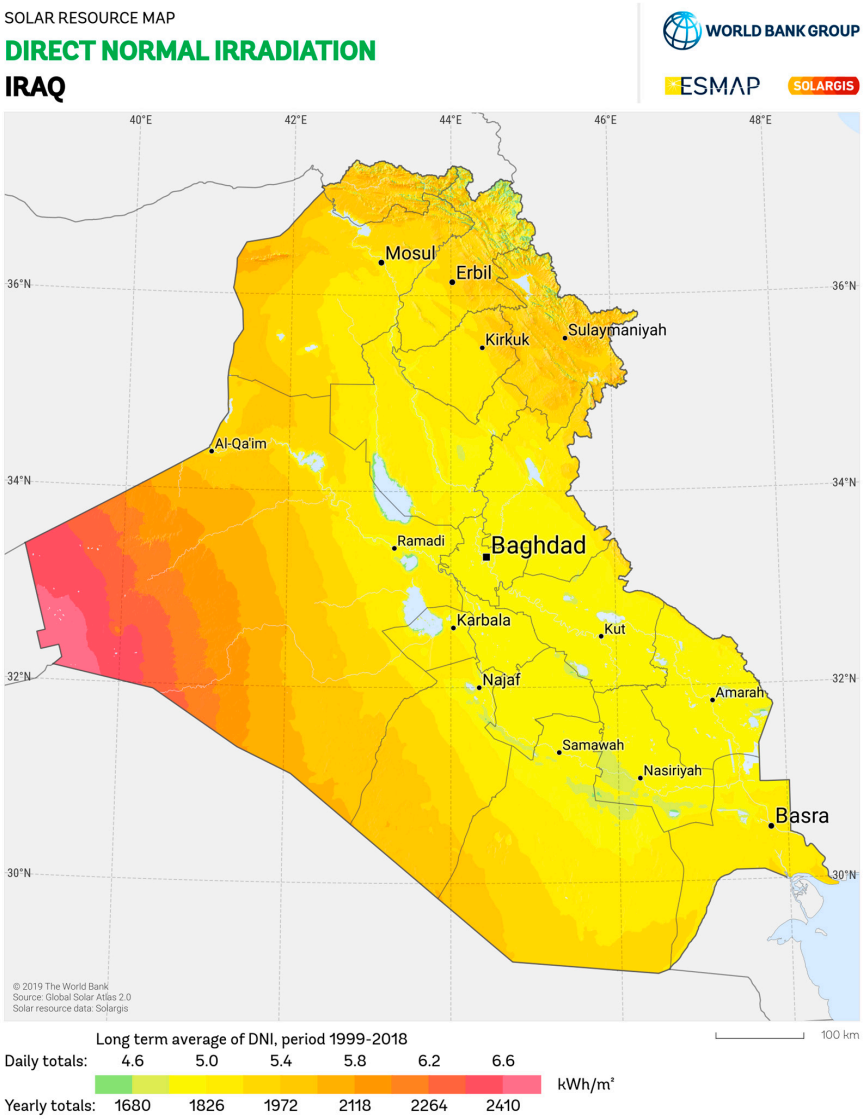

Figure 3. SOLARGIS global horizontal irradiation of location.

2.3.2. Define Plane Orientation

A fixed tilted plane is considered in this study. The filed parameters are azimuth of 0° and tilt of 45° to obtain maximum yield in winter; global irradiance calculated at this angle is 928 kWh/m^2.

2.3.3. PV Power Plant Design

In total, 102 TSM-DE18M(II) PV modules form the PV power plant, which has a total installed capacity of 51 kW. The specifications for PV module are represented in Table 6. The 102 modules are assembled into four units, and each unit is connected to a three-phase SUN-12K-SG04LP3 inverter having a rated output power of 15.6 kW. The specifications for the inverter are represented in Table 7. Each unit has two strings; three units have thirteen modules each, for a total of 26 modules per inverter, and one unit has twelve, for a total of 24 modules per inverter. The inverter's maximum power tracking voltage range is 800 V, and the Voc computed per string is 715.79 V for three units and 660.73 V for one unit. The combined Isc for each string is 12.28 A, which is less than the inverter's maximum PV short-circuit current range of 17 A.

Table 6. Specifications for PV module.

S.no	Parameter	Value	Unit
1	Maximum power (P max)	500	Watt
2	Maximum power voltage Vmpp	42.8	V
3	Open circuit voltage (V_{oc})	51.7	V
4	Short-circuit current (I_{sc})	12.28	A
5	Max power point	11.69	A
6	Total efficiency	20.9	%
7	Power warranty of 84.8% output power	25	Year

Table 7. Specifications for inverter.

S.no	Parameter	Value	Unit
1	Rating power of the inverter	13.2	kVA
2	DC voltage input	150–8000	V
3	Efficiency	97.6	%

2.3.4. Detailed Losses

In this design, thermal parameter is selected for modules with air circulation, ohmic losses for 2 × 16 m of 2× single-core 6 mm^2 DC cable per string and 10 m of four-core 10 mm^2, module quality is selected from specifications, LID loss factor as 2%, module mismatch losses as 2%, string voltage mismatch as 0.1%, and soiling losses as 3%.

2.3.5. Shading Analysis

The effect of far shading is neglected because no adjacent object is casting a shadow on the modules. For the geographic location, the height of the sun's elevation above the sky is essential, as it is understood that the lowest is on the winter solstice, i.e., in December. Figure 4 represents the solar elevation angle corresponding to the field coordinates. Depending on the geographic location—the hemisphere, zone, and the exact location expressed in degrees—the sun's height can be calculated as shown in Figure 5.

$$Height\ difference(h) = sin\ \theta \times L \quad (3)$$

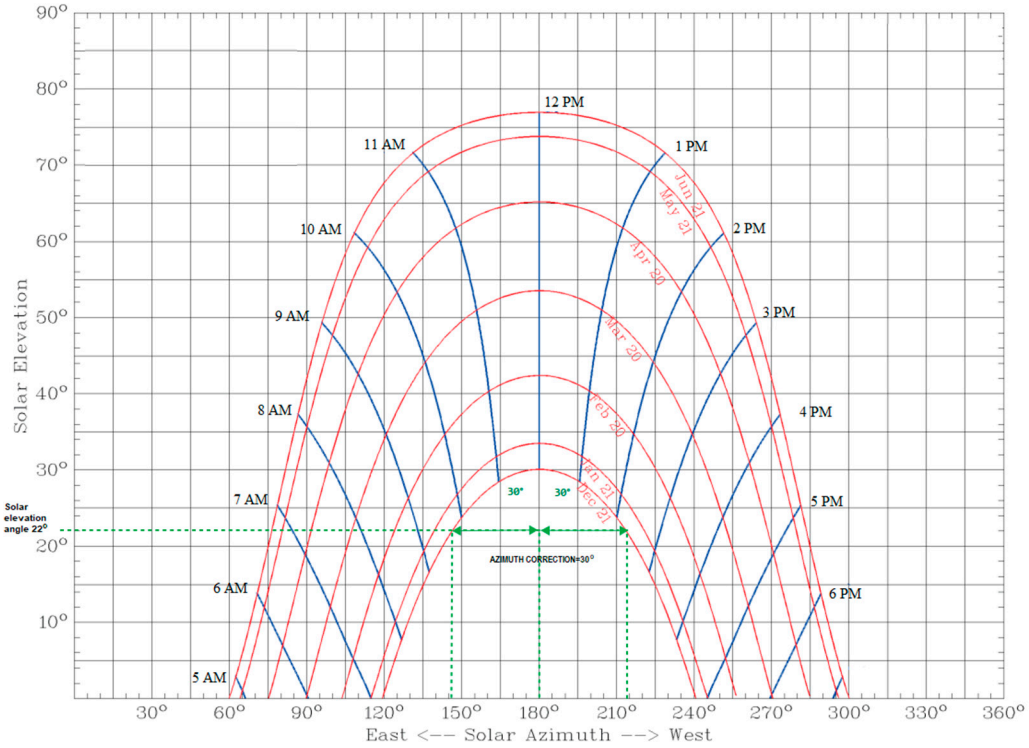

Figure 4. The solar elevation angle corresponds to the field coordinates.

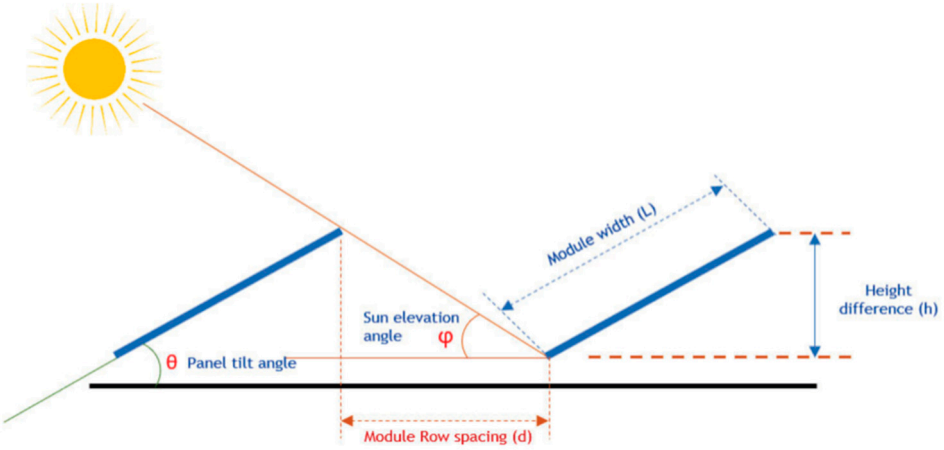

Figure 5. Shading calculation.

Here, θ is tilt angle (°) and L is module width (m). The selected solar panel width is 2.176 m. There are two panels in a module width; hence, the module width is 2 × 2.176 = 4.352 m.

$$Module\ shading\ length = \frac{h}{Atan\ \varphi} \tag{4}$$

Here, h is the height difference (m) and φ is the sun elevation angle (°) from the plot, the sun elevation angle for December 21st, and the picked-up time frame for 10 a.m. to 2 p.m. is 24°.

Further, the azimuth angle correction shall be considered to calculate the minimum row spacing (d). For this location, the calculated azimuth angle for December 21 is 30°.

$$d = Module\ shading\ length \times cos\ (\alpha) \tag{5}$$

Here, d is the minimum module shading length and α is the azimuth correction angle (reference from the sun elevation angle plot, Figure 4). Results of shading calculations are

shown in Table 8. Moreover, Figure 6 shows the architectural layout for the PV power plant at the site.

Table 8. Shading calculation results.

Tilt Angle (θ)	Module Width (L), m	Height Difference (h), m	Module Shading Length, m	Azimuth Correction Angle (a), °	Minimum Module Shading Length (d), m
Equation		3	4		5
45	4.352	3.091	6.942	30	6.0

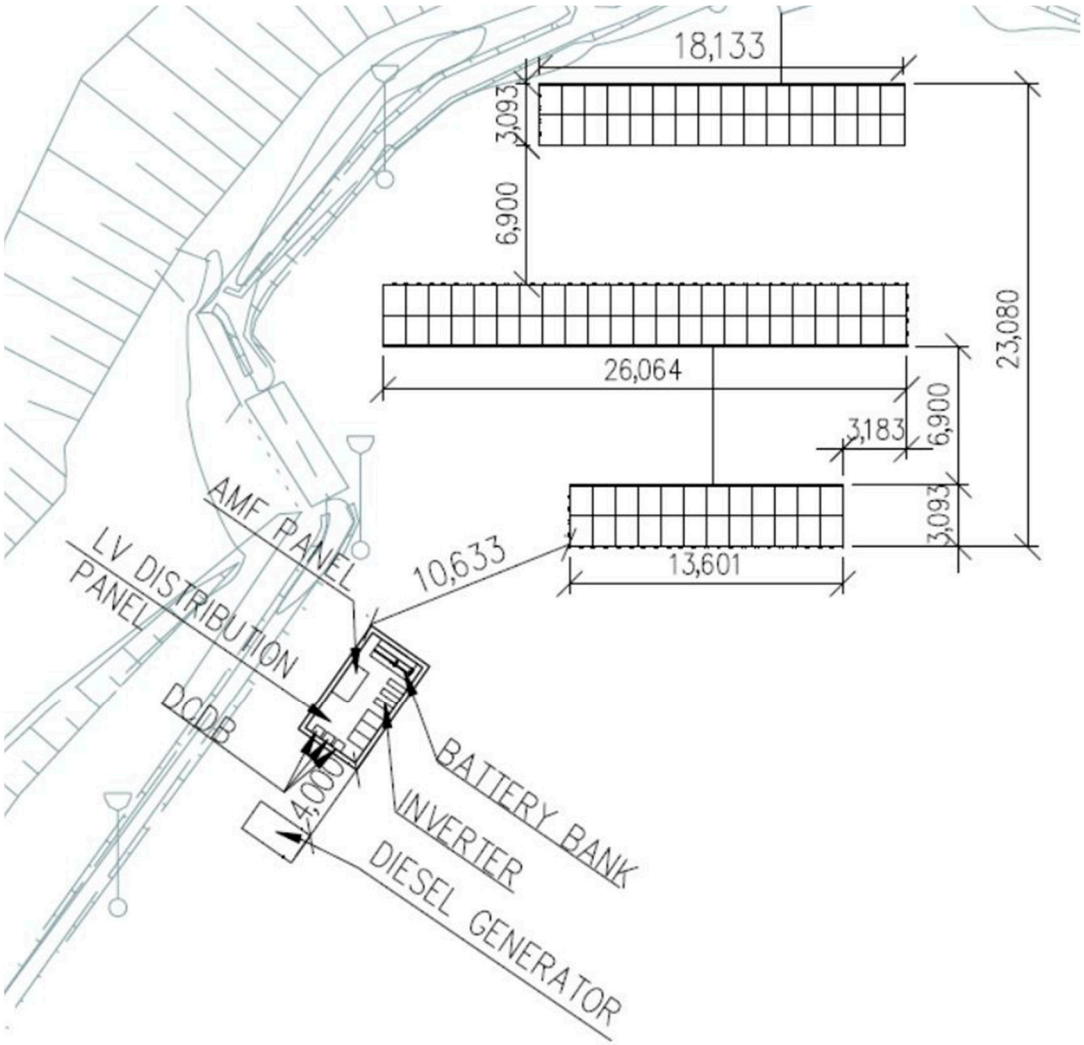

Figure 6. Architectural layout for the PV power plant.

2.4. Designing the Hybrid Stand-Alone Microgrid

The HOMER Pro version 3.14.2 software has many advantages and is utilized for the hybrid stand-alone microgrid model's planning, design, and optimization. These advantages include its capacity to accommodate various renewable energy resources and several other elements needed for the reliable hybrid stand-alone microgrid model. The software is quite competent in determining the model's economic and technological viability. The flowchart for designing the hybrid stand-alone microgrid using HOMER Pro software is shown in Figure 7. The HOMER Pro software imports the PV plant's CSV file from the PVsyst software for better results.

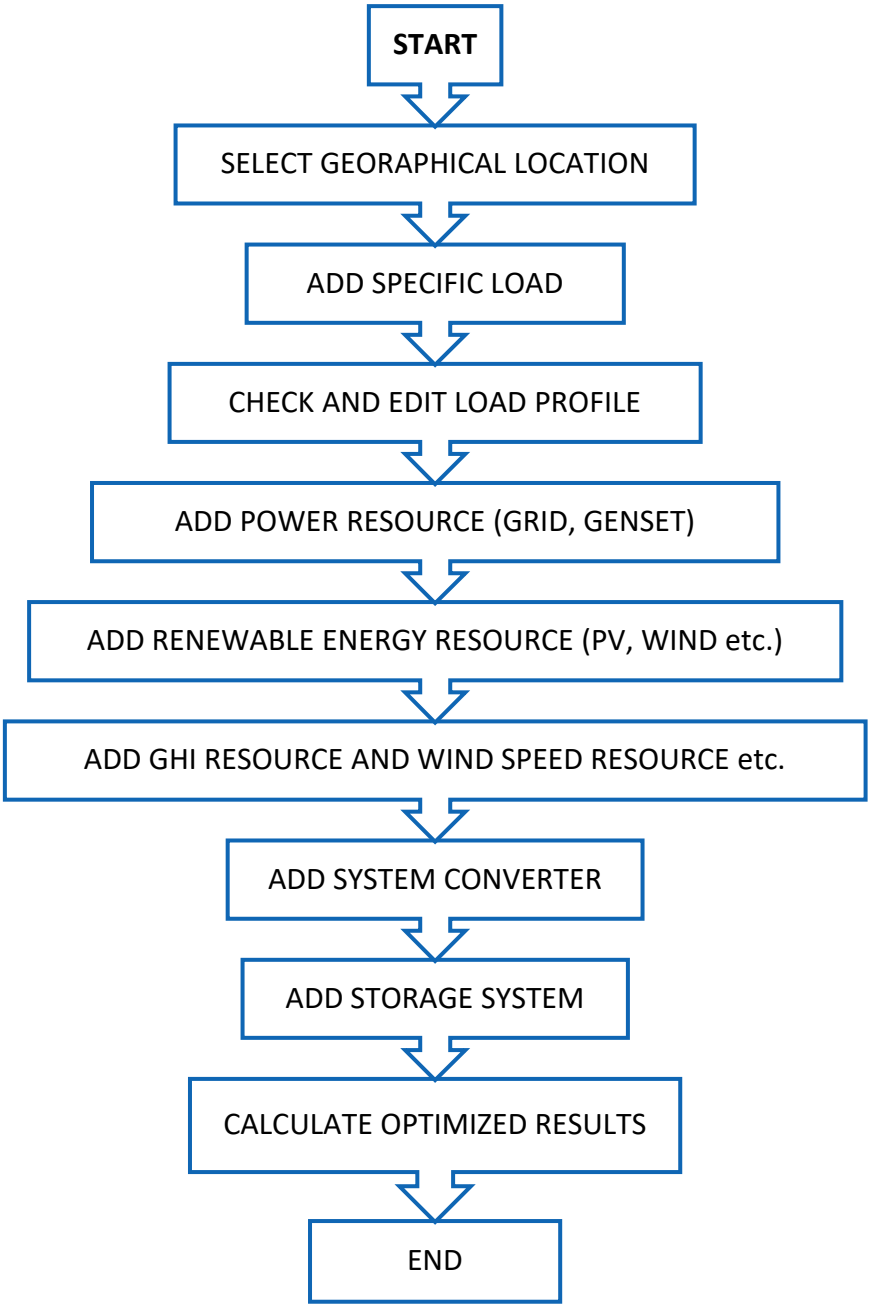

Figure 7. Flowchart for designing the hybrid stand-alone microgrid using HOMER Pro software.

Moreover, Figures 8–10 shows schematics of the connection diagram for several hybrid stand-alone microgrid components, including the configurations for the DC distribution box, inverter, AC distribution box, BESS, load, and EDG of the proposed hybrid stand-alone microgrid network. Figure 8 represents the schematics of DCDBs and inverters' connection configuration, Figure 9 represents the schematics of BESS and inverters' connection configuration, and Figure 10 represents the schematics of AC side connection configuration.

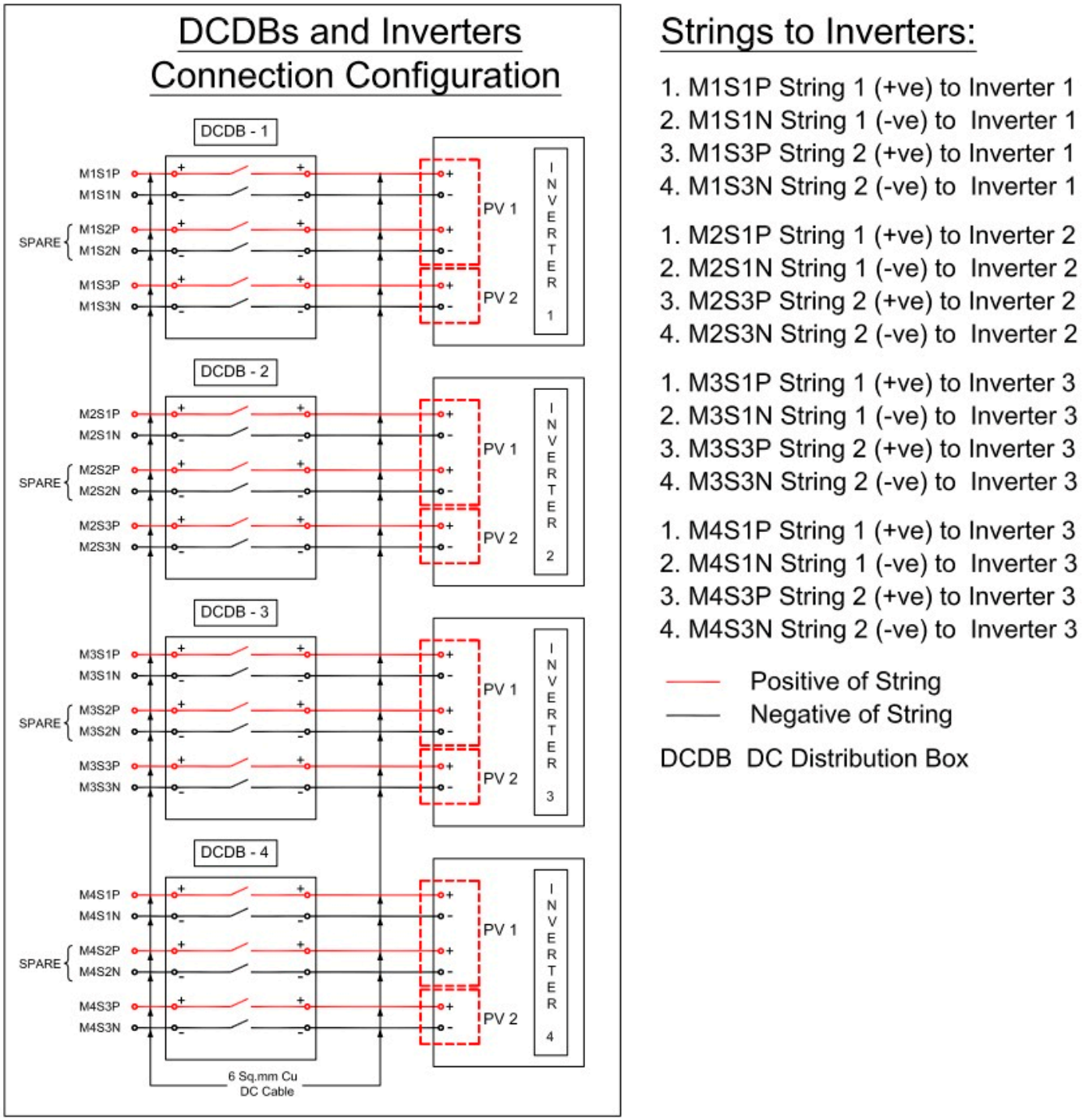

Figure 8. Schematics of DCDBs and inverters' connection configuration.

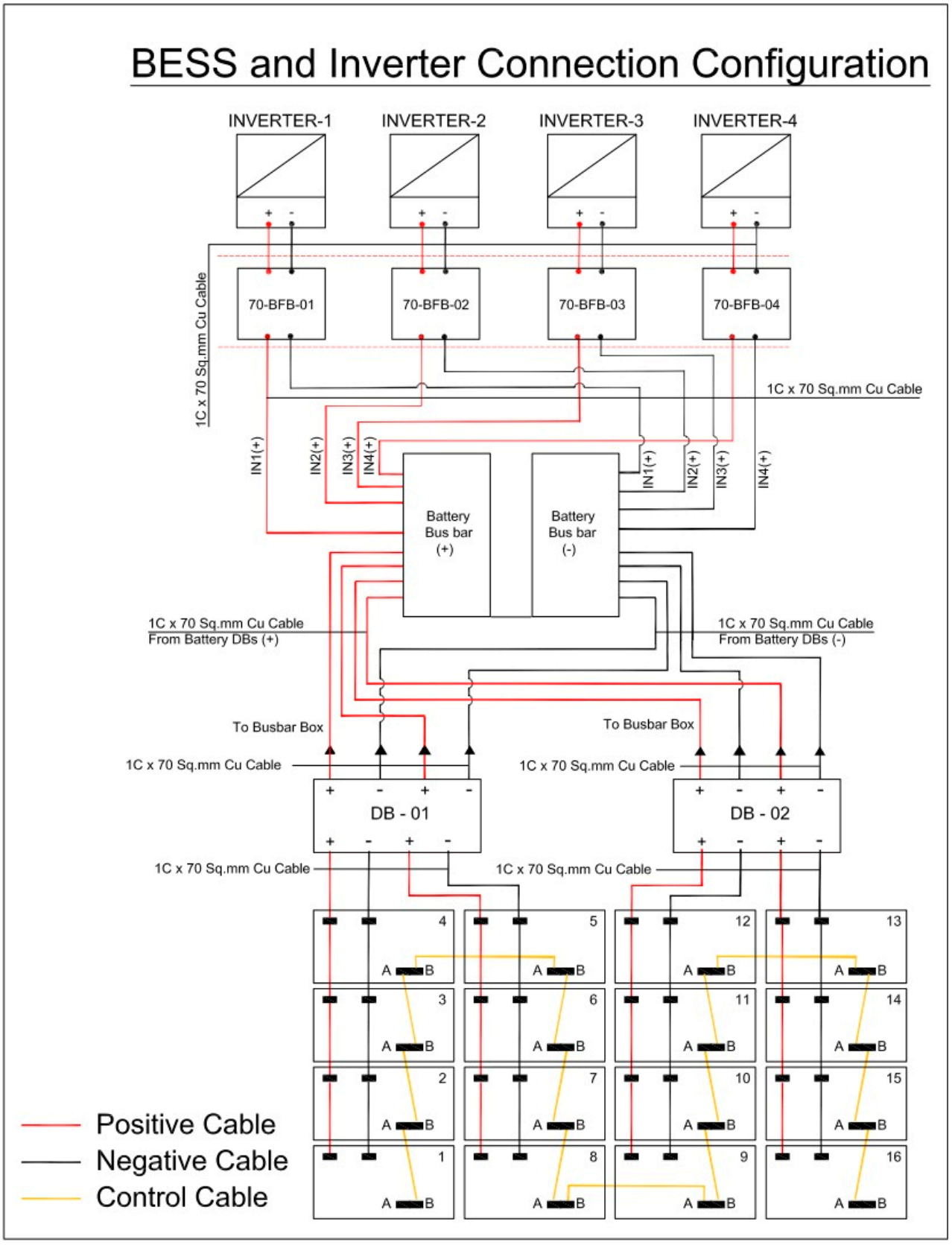

Figure 9. Schematics of BESS and inverters' connection configuration.

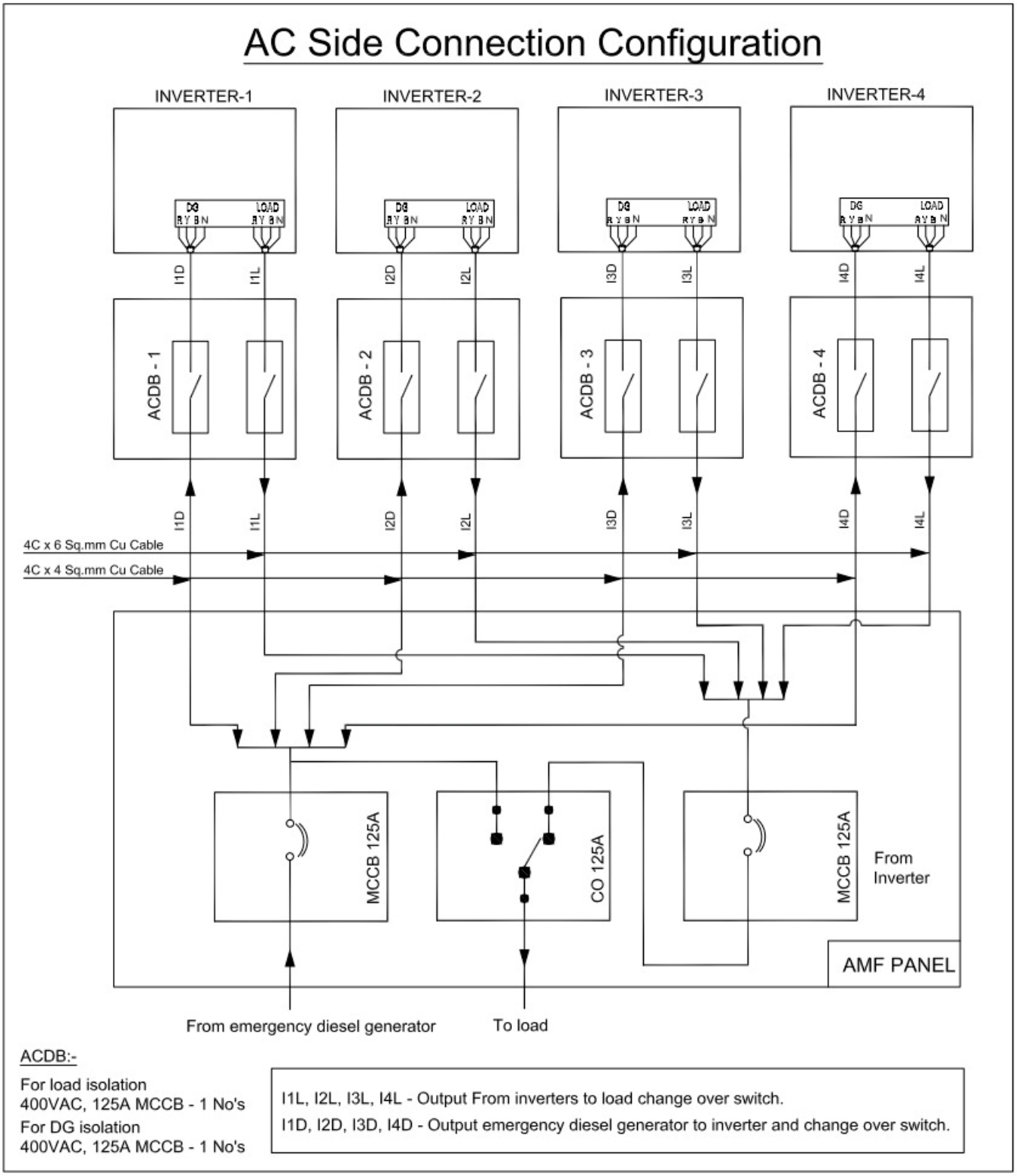

Figure 10. Schematics of AC side connection configuration.

2.5. Performance Analysis of Hybrid Stand-Alone Microgrid

SAM (System Advisor Model) version 2020.11.21 software is used to analyze proposed hybrid stand-alone microgrid's performance. SAM software offers detailed insights into the energy production, consumption, and storage within the microgrid system. SAM is used to assess the proposed hybrid stand-alone microgrid system's overall effectiveness,

viability, and reliability. For the performance analysis of the microgrid in this study, SAM (System Advisor Model) software is used. Figure 11 depicts a flowchart for BESS charging, and Figure 12 depicts a flowchart for BESS charging using SAM software.

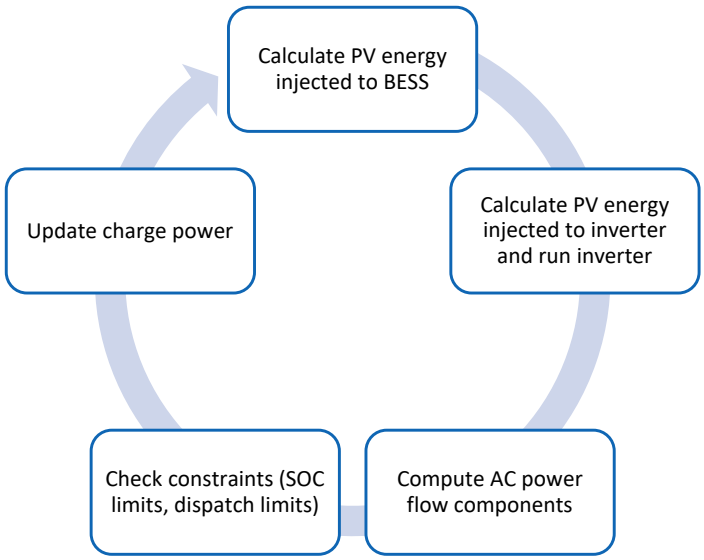

Figure 11. Flowchart for BESS charging.

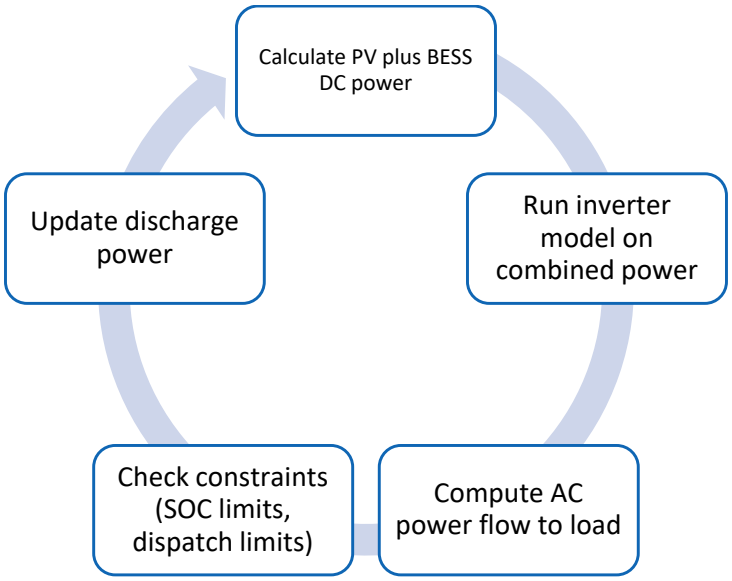

Figure 12. Flowchart for BESS discharging.

3. Results and Discussions

The first part of this section discusses the projected PV power plant's results as determined by the PVsyst software. The second part of this section discusses the results of the proposed hybrid stand-alone microgrid that was produced using the HOMER Pro software. The performance analysis findings from the SAM (System Advisor Model) software for the proposed hybrid stand-alone microgrid are covered in the third part. The final part of this section discusses the findings of the installed hybrid stand-alone microgrid's site testing.

The purpose of this study is to determine the best solution to design and implement a hybrid stand-alone microgrid; therefore, different software is used in combination as each software has its own benefits and limitations.

3.1. PV Power Plant's Results

A PV power plant's performance is typically analyzed using a set of performance characteristics defined by IEC Standard 61724 [31–33]; nevertheless, the most important parameters include final energy output, performance ratio, and capacity factor. These parameters provide information about the system's energy production, the utilization of available solar resources, and the overall effect of system losses.

The quantity of AC power produced by the system over a certain period is defined as the final energy output of a PV power plant. The total energy produced can be calculated using IEC Standard 61724:

$$E_{AC} = \sum_{t=1}^{N} E_{AC(t)} \quad (6)$$

where EAC (kWh) is the final energy output at time t, and N represents the number of data sets. In the context of bifacial photovoltaic (PV) modules, the elevation of the module holds significant implications for their performance. Elevating the modules heightens backside irradiance uniformity, thereby amplifying bifacial power gain. This enhancement is attributed to an augmented perception of ground-reflected light on the rear side of the PV modules. Moreover, by manipulating ground albedo, the reflective nature of the surface, an additional avenue for optimizing bifacial power gain is unveiled. A heightened ground albedo intensifies the perception of ground-reflected light on the backside of the PV modules, further contributing to increased energy generation. To illustrate these phenomena, Figure 13 delineates the impact of ground clearance on annual generation across various tilt angles of PV modules, while Figure 14 illustrates the influence of ground albedo on annual generation, considering a scenario of zero ground clearance. These figures serve as visual representations of the intricate interplay between module height, ground clearance, albedo, and the ensuing impact on bifacial PV module performance.

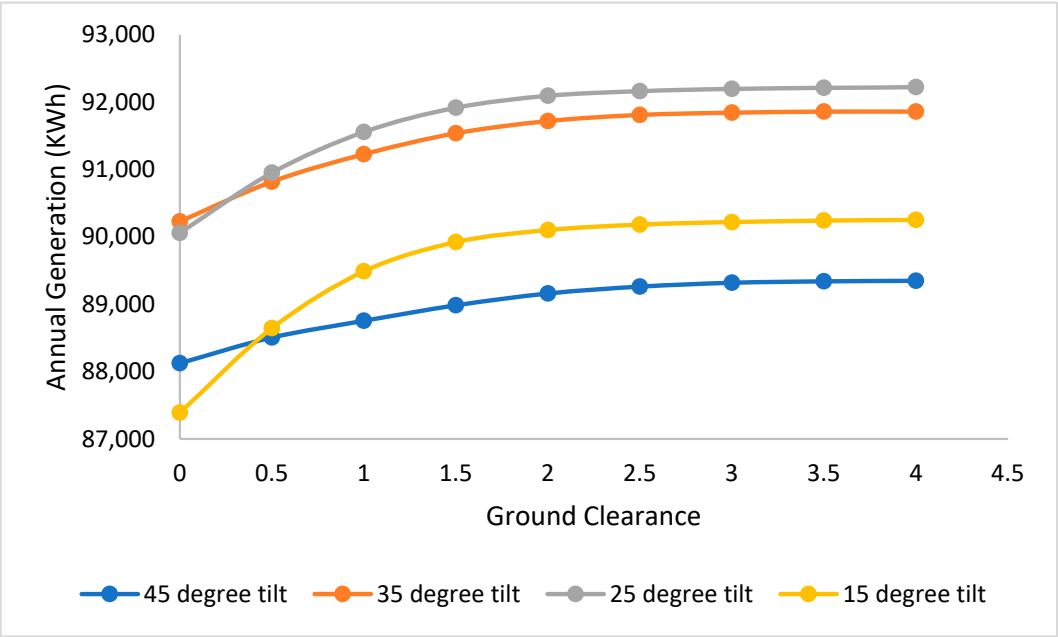

Figure 13. Impact of ground clearance on annual generation across various tilt angles of PV modules.

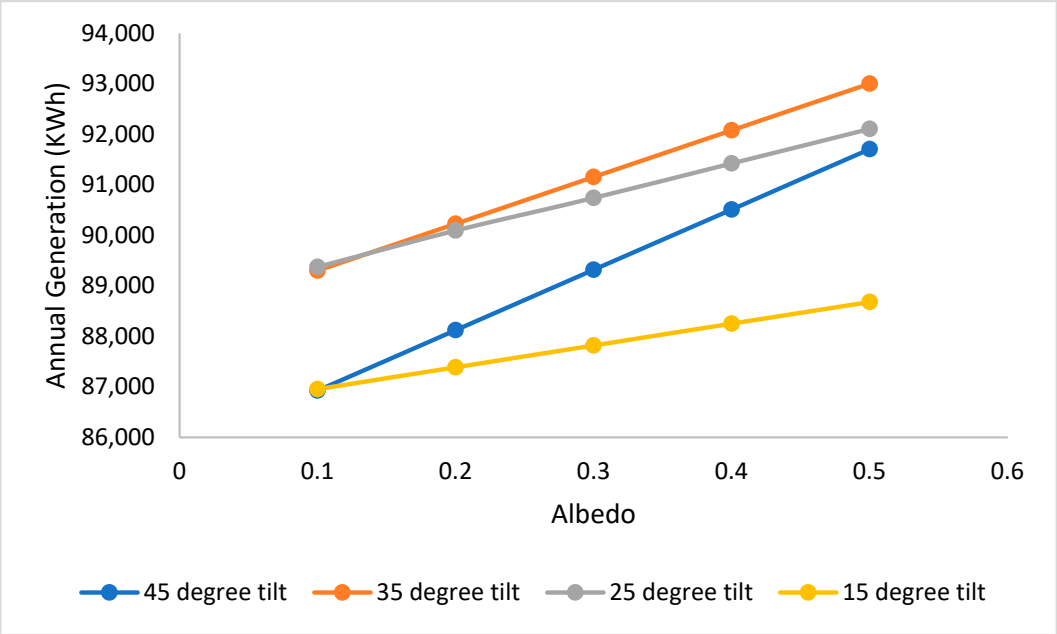

Figure 14. Impact of ground albedo on annual generation across various tilt angles of PV modules considering zero ground clearance.

For monofacial PV modules, which are used in the proposed microgrid, Figure 15 depicts the PVsyst-software-determined daily system output energy of the proposed PV plant. Figure 16 shows the normalized productions per installed kWp of PV plant, with a collecting loss of 0.92 kWh/kWp/day, a system loss of 0.11 kWh/kWp/day, and a usable energy output of 4.53 kWh/kWp/day.

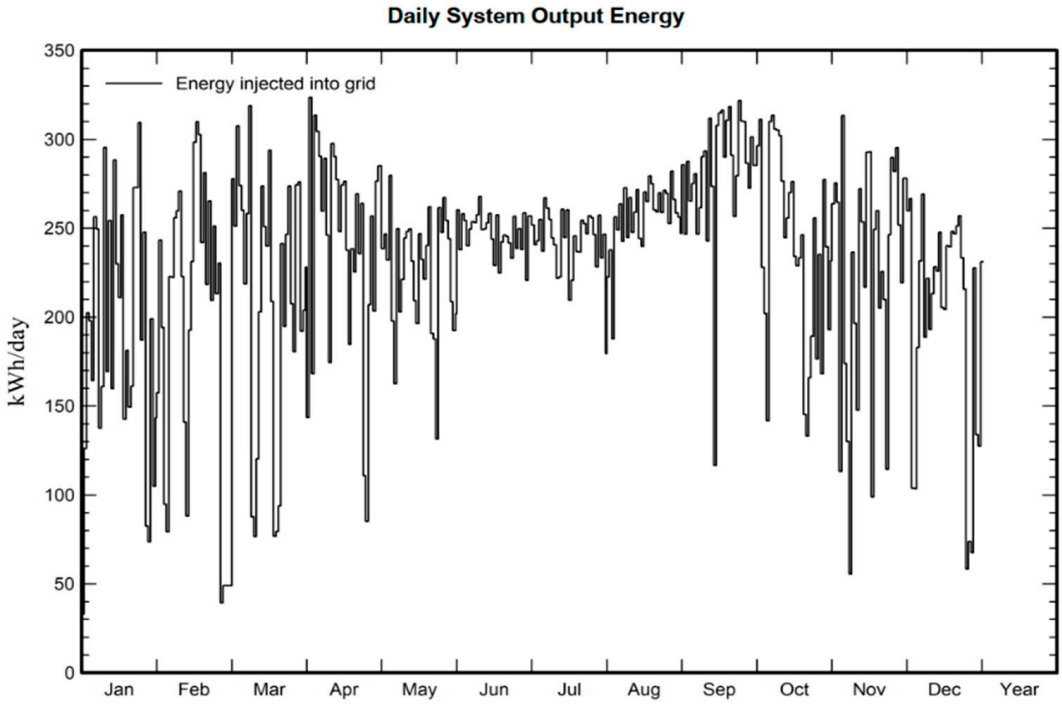

Figure 15. Daily system output energy of PV plant.

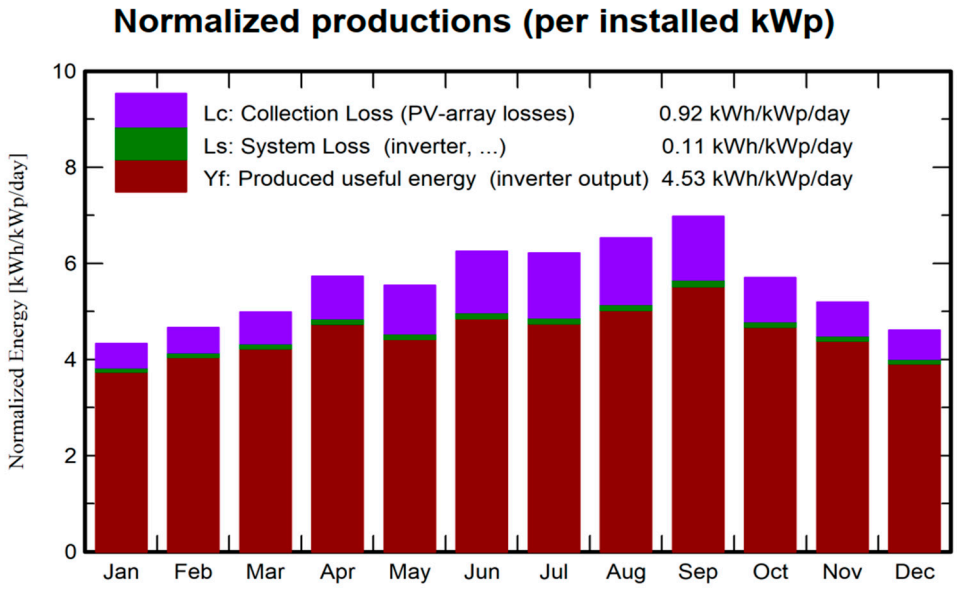

Figure 16. Normalized productions per installed kWp of PV plant.

Figure 17 presents the loss analysis of the PV plant for a year. Furthermore, Figure 18 depicts the probability distribution for the PV plant, with the 50th percentile value (P50) indicating that the probability of annual energy production is 84.31 MWh, the 90th percentile value (P90) indicating that the probability of energy production is 79.57 MWh, and the 95th percentile value (P95) indicating that the probability of energy production is 78.24 MWh.

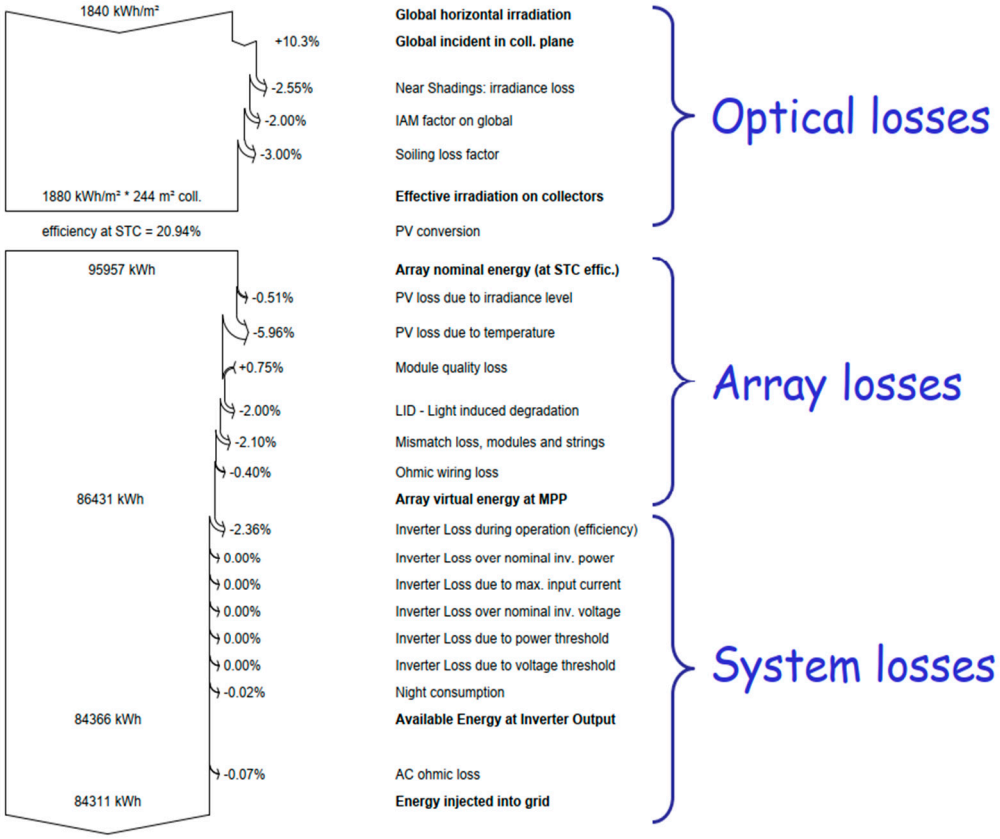

Figure 17. Loss analysis of PV plant.

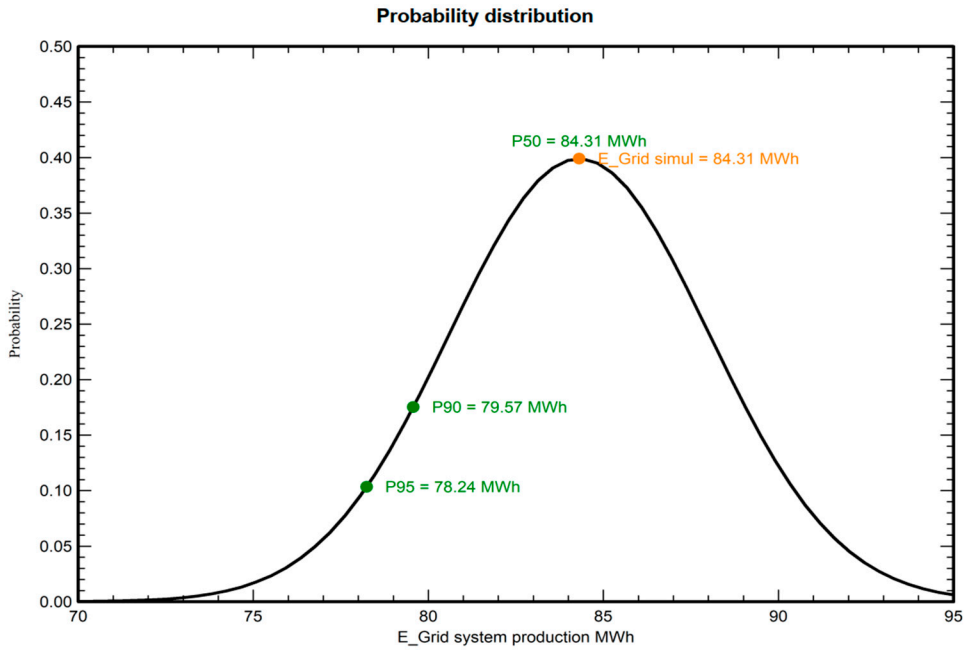

Figure 18. Evaluation of probability distribution.

The performance ratio (PR) of a PV power plant assesses the overall impact of losses on the system's rated output and shows how closely its performance adheres to ideal performance under actual operating conditions. The reference is IEC Standard 61724:

$$PR = \frac{E_{AC}}{P_{PV-rated}} \times \frac{G_{STC}}{H_{POA}} \quad (7)$$

where $P_{PV-rated}$ is the installed capacity (in kW) of the PV system, H_{POA} is the in-plane array radiation (in kWh/m^2/day), and G_{STC} is the reference irradiance (in kW/m^2). Figure 19 shows the projected PV plant's performance ratio (PR), which was calculated using the PVsyst software and is 81.5%.

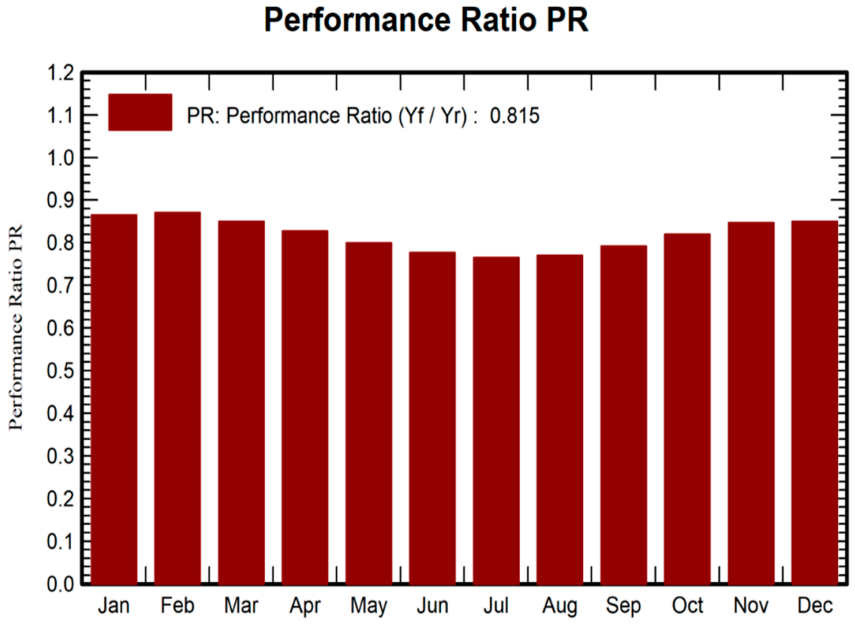

Figure 19. Performance ratio (PR) of PV plant.

A solar PV installation's capacity factor is calculated as the difference between the total energy it produces over a certain period and the amount of energy it would have produced if it had been operating at full capacity throughout the period. For instance, the annual capacity factor is stated as follows:

$$C_f = \frac{E_{AC(a)}}{P_{PV-rated} \times A_h} \quad (8)$$

where $E_{AC(a)}$ is the total yearly final energy generated, and A_h is the total predicted number of operating hours in a particular period, usually taken to be a year.

$$C_f = \frac{84311\ kWh}{51\ kW \times 365 \times 5.5\ h} = 0.82$$

A solar PV panel installation will decrease CO_2 emissions, which will contribute to a pollution-free environment. In Figure 20, the green line represents the amount of carbon emissions saved, which is 1811.6 tons of carbon emissions expected by the simulation over the next 30 years are saved.

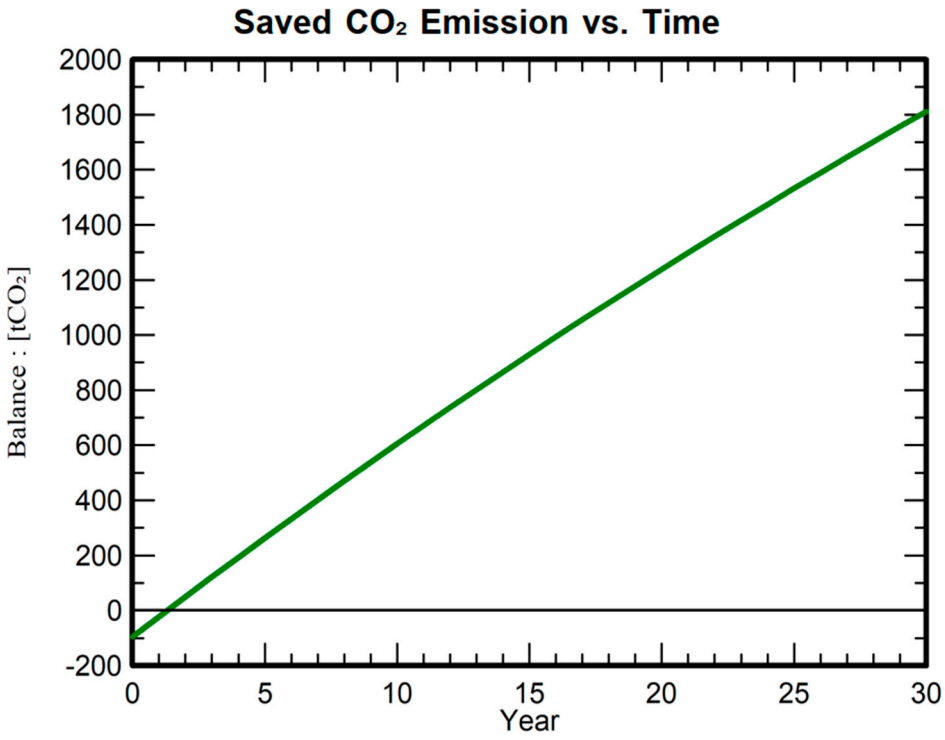

Figure 20. Saved CO_2 emissions for the next 30 years.

3.2. Proposed Hybrid Stand-Alone Microgrid's Results

This section discusses the results of the HOMER Pro software simulation for the proposed hybrid stand-alone microgrid. Figure 21 shows the predicted power injection from the PV plant to the hybrid stand-alone microgrid, with vertical blurred blue lines at the beginning and conclusion of the picture indicating a lack of power supply to meet the load, dark blue area indicates 0% injection, light blue area indicates 25–50% injection, green area indicates 50–75% injection, and yellow area indicates 100% power injection, while Figure 22 shows the predicted power injection from the EDG to the hybrid stand-alone microgrid for the entire year, with yellow areas indicating power injection from the EDG to the microgrid and dark blue area indicates 0% injection from the EDG to microgrid. Additionally, Figure 23 depicts the expected PV plant and EDG output for the entire year to meet load demand. It may appear that in the months of November, December, and January, PV generation is insufficient to meet load needs; hence, EDG is used to meet load demand.

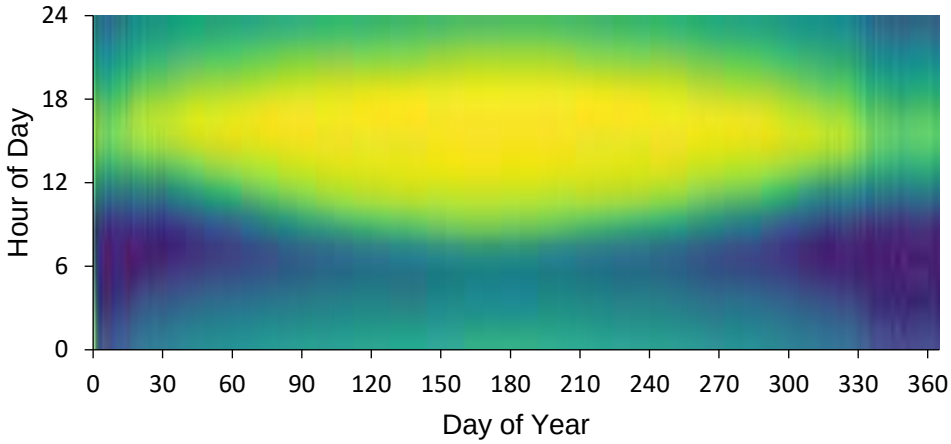

Figure 21. Power injection from the PV plant.

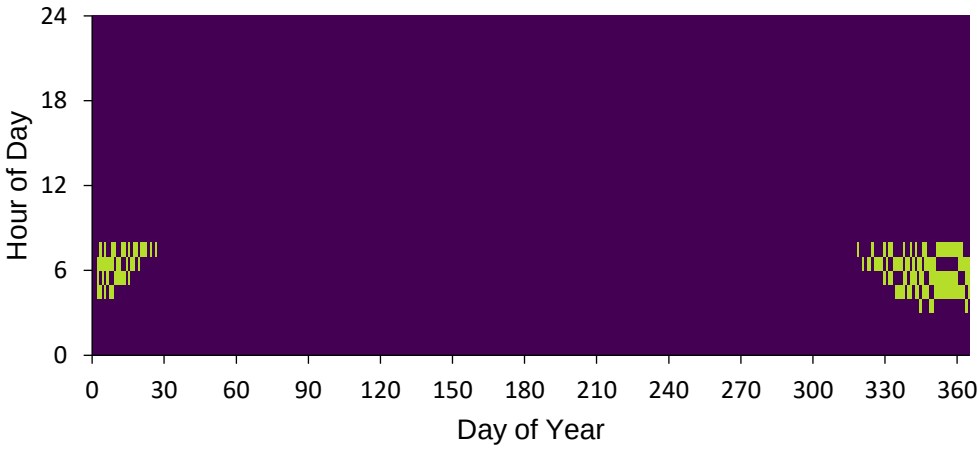

Figure 22. Power injection from the EDG.

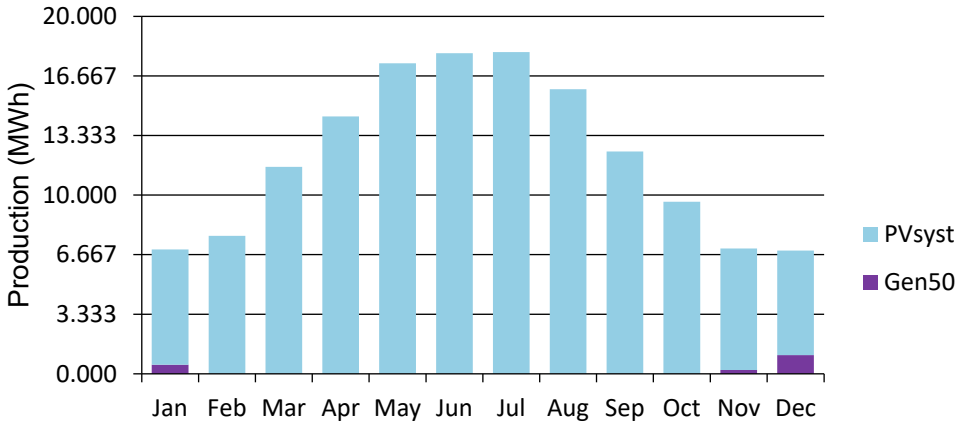

Figure 23. Expected PV plant and EDG output for the entire year.

3.3. Performance Analysis Results of Proposed Hybrid Stand-Alone Microgrid

This section discusses the SAM software simulation's performance analysis results for the proposed hybrid stand-alone microgrid. The hybrid stand-alone microgrid's performance analysis results are pretty excellent. Figure 24 depicts the simulated BESS charge (Ah) level, energy injected from the microgrid to charge the BESS, and discharging of the BESS to fulfill load demand for each month of the year. Figure 25 depicts the simulation results of the BESS's state of charge (SOC), energy injected from the microgrid to charge the BESS, and discharging of the BESS to fulfill load demand for each month of the year. Figure 26 shows the simulation results of unmet critical load, energy injected from the

microgrid to charge the BESS, and discharging of the BESS to fulfill load demand for each month of the year. These comprehensive analyses shed light on the hybrid microgrid system's performance and efficiency.

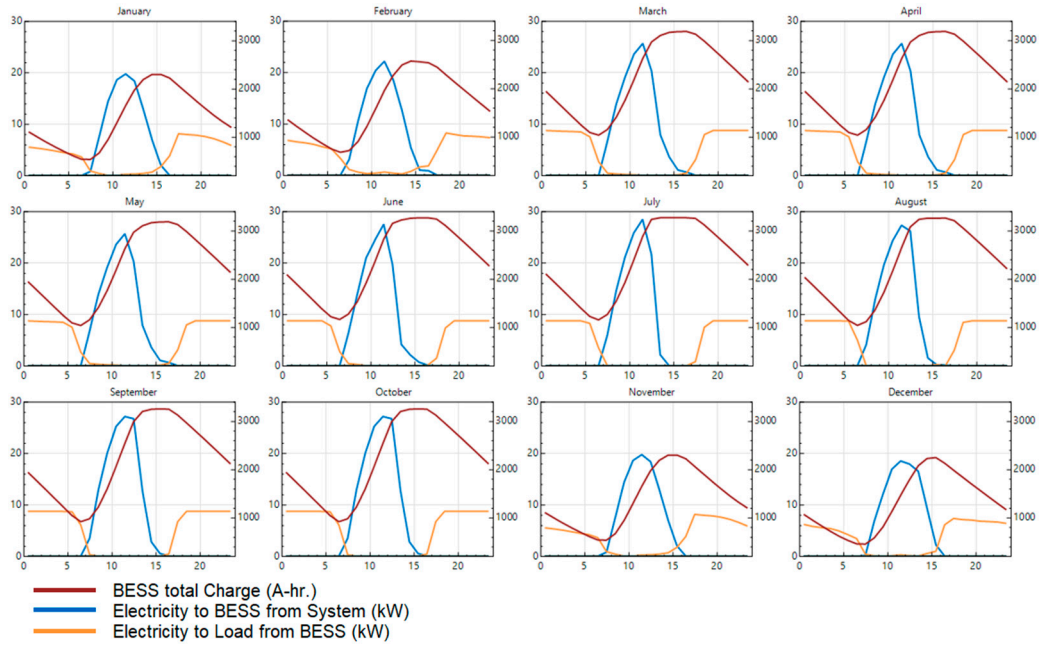

Figure 24. BESS charge (Ah) and discharge level.

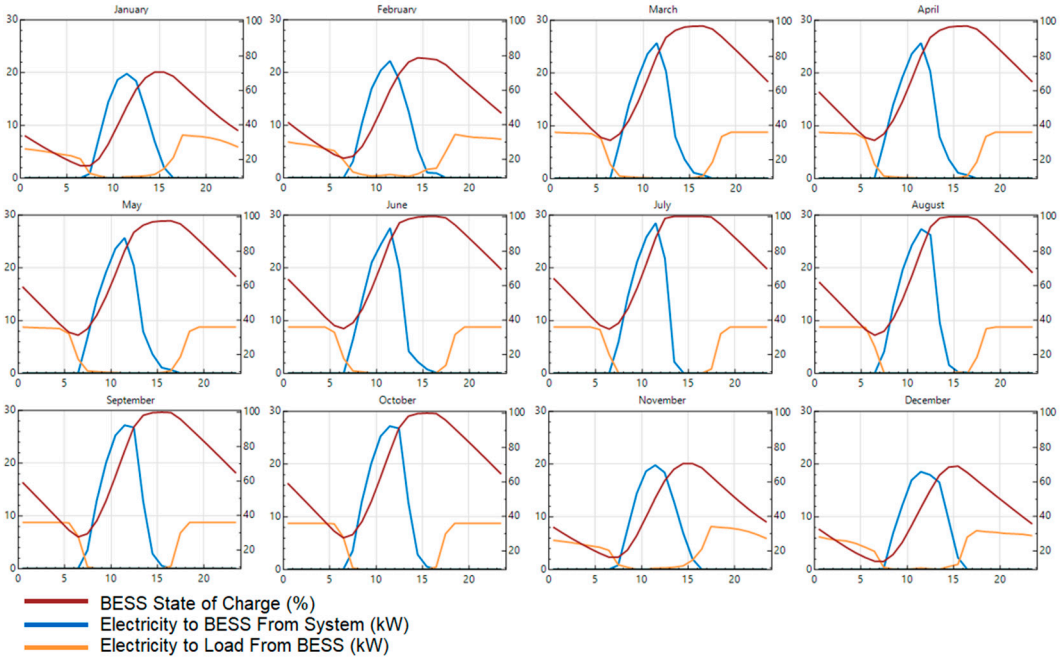

Figure 25. BESS state of charge (%), charging, and discharge.

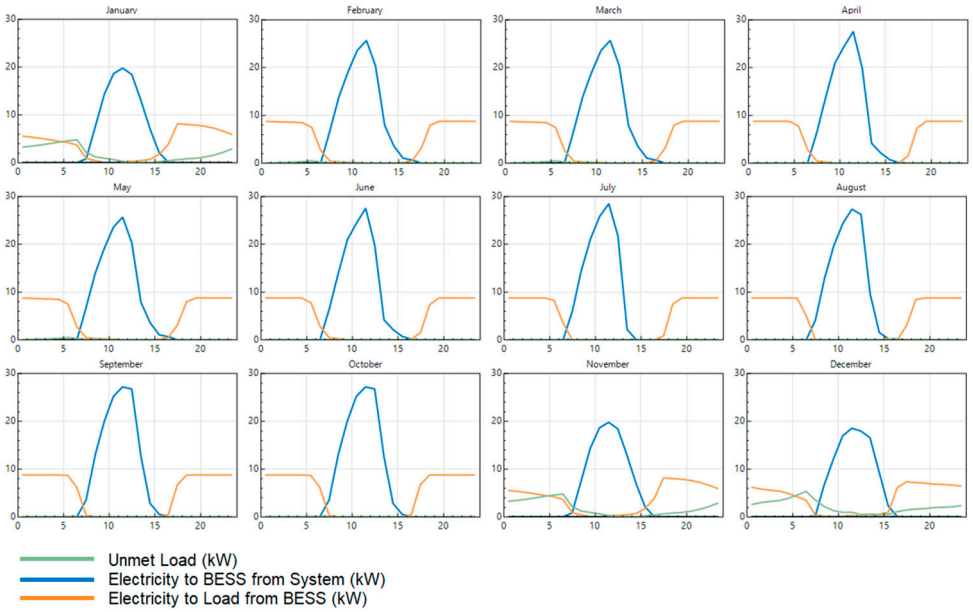

Figure 26. Unmet load, BESS charging, and discharge.

The results obtained from the software analysis have yielded satisfactory outcomes, thus validating the feasibility of implementing the same design in experiment.

3.4. Experimental Results

This section covers the site testing's findings and an overview of hybrid stand-alone microgrid generation and consumption for August. Table 9 provides the results for DC string voltage, showcasing the voltage levels across the strings. Table 10 shows the battery bank results, which reveal important information about the battery's performance. Moving on to Tables 11 and 12, they present the load test results for both the inverters and the battery, specifically at a 10.5 kW load. Lastly, Appendix A presents the testing results of the hybrid stand-alone microgrid on an hourly basis, providing valuable insights into its performance throughout the day. Moreover, Figure 27 presents the summary of hybrid stand-alone microgrid generation and consumption for the month of August. Analyzing these results will help us evaluate the efficiency and effectiveness of the system.

Table 9. DC string voltage.

String No.	Panels/String	Irradiance (W/m^2)	Rated Voltage (Vmpp)	Recorded Voltage (Vmpp)
1	13	775	672	608.6
2	13	775	672	610.6
3	13	763	672	607.1
4	13	763	672	606.8
5	13	766	672	604.9
6	13	765	672	605.2
7	12	760	620	557.6
8	12	765	620	556.8

Table 10. Battery bank results.

Battery No.	Rated Voltage (V)	Capacity (Ah)	Recorded Voltage (V)
1	48	200	49.69
2	48	200	49.79
3	48	200	49.82
4	48	200	49.86

Table 10. *Cont.*

Battery No.	Rated Voltage (V)	Capacity (Ah)	Recorded Voltage (V)
5	48	200	49.85
6	48	200	49.87
7	48	200	49.86
8	48	200	49.9
9	48	200	49.88
10	48	200	49.89
11	48	200	49.9
12	48	200	49.93
13	48	200	49.92
14	48	200	49.91
15	48	200	49.93
16	48	200	49.91

Table 11. Load test for the inverters.

Load Test with Solar Production 9 a.m.					
Connected Load (kW)		10.5	Irradiance (W/m^2)		802
Inverter No.	PV Power (W)	Battery SOC (%)	Vac (V)	Load Iac (A)	P (kW)
Master-01	6208	76	410	5.6	2398
Slave-02	6184	76	410	6.1	2530
Slave-03	5751	76	410	6.3	2701
Slave-04	6208	77	410	6.3	2765
Load test with solar production 9 p.m.					
Connected Load (kW)		10.5	Irradiance (W/m^2)		0
Inverter No.	PV Power (W)	Battery SOC (%)	Vac (V)	Load Iac (A)	P (kW)
Master-01	0	25	410	6.3	2704
Slave-02	0	25	410	6.1	2522
Slave-03	0	25	410	6.3	2401
Slave-04	0	24	410	6.3	2763

Table 12. Load test for the batteries.

B-1	S.O.C (%):	83.56	B-5	S.O.C (%):	85.81	B-9	S.O.C (%):	84.96	B-13	S.O.C (%):	86.61
	Pack V:	49.55		Pack V:	49.56		Pack V (V):	49.56		Pack V:	49.61
	Im (A):	−9.1		Im (A):	−14.9		Im (A):	−14.82		Im (A):	−12.32
	Temp (C):	24.1		Temp (C):	24.5		Temp (C):	24.5		Temp (C):	24.6
B-2	S.O.C (%):	85.9	B-6	S.O.C (%):	87.03	B-10	S.O.C (%):	84.19	B-14	S.O.C (%):	86.59
	Pack V:	49.6		Pack V:	49.85		Pack V:	49.56		Pack V:	49.58
	Im (A):	−15.1		Im (A):	−12.8		Im (A):	−14.67		Im (A):	−13.29
	Temp (C):	24.3		Temp (C):	23.1		Temp (C):	22.6		Temp (C):	23.8
B-3	S.O.C (%):	87.8	B-7	S.O.C (%):	86.51	B-11	S.O.C (%):	85.55	B-15	S.O.C (%):	84.81
	Pack V:	49.6		Pack V:	49.65		Pack V (V):	49.6		Pack V:	49.57
	Im (A):	−13.7		Im (A):	−11.1		Im (A):	−13.73		Im (A):	−18.97
	Temp (C):	24.2		Temp (C):	24		Temp (C):	23.2		Temp (C):	23.1
B-4	S.O.C (%):	89.61	B-8	S.O.C (%):	82.9	B-12	S.O.C (%):	85.21	B-16	S.O.C (%):	82.44
	Pack V:	48.05		Pack V:	49.51		Pack V:	49.56		Pack V:	49.56
	Im (A):	−14.9		Im (A):	−15.9		Im (A):	−13.69		Im (A):	−15.58
	Temp (C):	24.9		Temp (C):	23.9		Temp (C):	24.2		Temp (C):	24.2

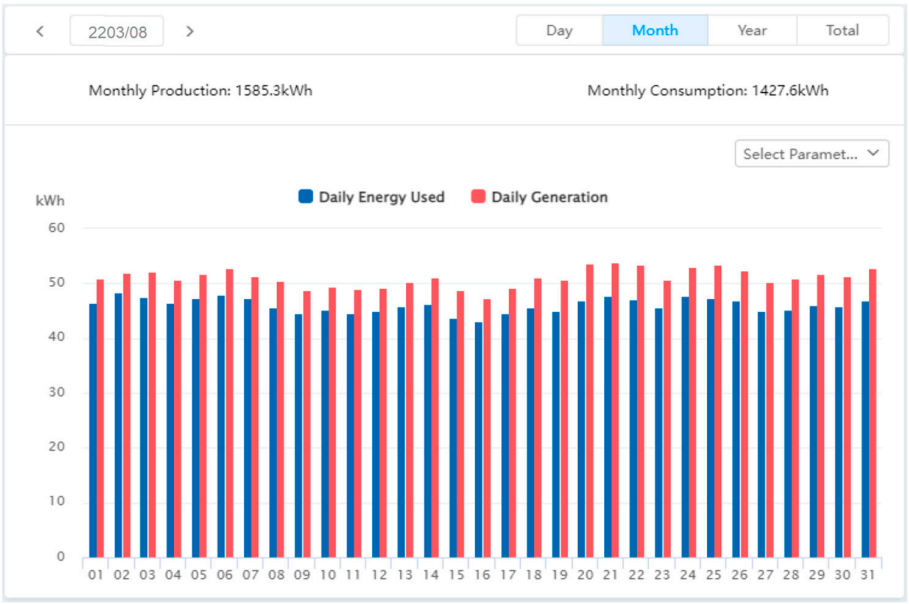

Figure 27. Summary of hybrid stand-alone microgrid generation and consumption.

4. Conclusions

This research article comprehensively analyzes a hybrid stand-alone microgrid system comprising PV modules, inverters, a battery storage system, a generator, and an AC load. Integrating PVsyst, HOMER Pro, and SAM software tools allowed for a thorough design, optimization, and performance evaluation of the hybrid stand-alone microgrid. The findings reveal increasing ground clearance results in uniform backside irradiance, which amplifies bifacial power gain to an optimal level, and increasing ground albedo also results in bifacial power gain. For monofacial power generation there was a promising normalized production of 4.53 kWh/kWp/day with a performance ratio of 0.815 and annual energy production estimates of 84.31 MWh (P50), 79.57 MWh (P90), and 78.24 MWh (P95). Notably, this study highlights the operational challenges faced during the winter months, necessitating generator support for load fulfillment. Moreover, the hybrid stand-alone microgrid is shown to be environmentally beneficial, saving approximately 1811.6 tons of CO_2 emissions over a 30-year period, emphasizing its positive impact on sustainability and clean energy initiatives. Furthermore, the successful installation and validation of the hybrid stand-alone microgrid through experimental testing underscore its practical applicability. This research contributes valuable insights to the field of hybrid stand-alone microgrid design and underscores the importance of hybrid energy solutions to ensure a reliable power supply under varying conditions while simultaneously mitigating greenhouse gas emissions. This research will assist researchers/engineers/designers in optimizing, modeling, performance evaluating, designing, and implementing microgrid components while taking into account various parameters.

Author Contributions: Conceptualization, A.S. and M.Z.A.B.; methodology, M.Z.A.B.; software, M.Z.A.B.; validation, A.S., S.A. and W.A.; formal analysis, W.A.; investigation, A.S.; writing—original draft preparation, M.Z.A.B.; writing—review and editing, W.A.; supervision, A.S.; project administration, S.A. All authors have read and agreed to the published version of the manuscript.

Funding: This research received no external funding.

Data Availability Statement: Data are contained within the article.

Acknowledgments: The authors of the article appreciate the referees for their valuable suggestions, which contributed to improving the paper.

Conflicts of Interest: The authors declare no conflicts of interest.

Appendix A Hourly Basis Testing Results of the Hybrid Stand-Alone Microgrid

	Time:	7:00	8:00	9:00	10:00	11:00	12:00	13:00	14:00	15:00	16:00	17:00	18:00	19:00	20:00	21:00	22:00	23:00	0:00	1:00	2:00	3:00	4:00	5:00	6:00
Irradiance (W/m^2):		82	390	525	802	870	912	910	815	620	490	102	50	0	0	0	0	0	0	0	0	0	0	0	0
INV-1	**PV P(W):**	912	3872	6208	2507	2458	2582	2445	2456	2405	2539	2020	234	219	2	10	0	3	11	0	0	0	6	48	204
	Load P(W):	2039	2326	2398	2644	2556	2775	2704	2636	2728	2494	2452	2426	2333	2328	2448	1951	2262	2822	2562	2827	2310	2483	2544	2505
	EDG P(W):	-	-	-	-	-	-	-	-	-	-	-	-	-	-	-	-	-	-	-	-	-	-	-	-
INV-2	**PV P(W):**	853	3875	6184	2693	2672	2681	2624	2714	2721	4260	1954	369	29	0	0	0	0	0	0	0	0	0	76	228
	Load P(W):	2318	2151	2530	2658	2658	2650	2781	2617	2669	2329	2591	2463	2556	218	2300	2553	2534	2822	2331	2375	1883	2176	2308	2370
	EDG P(W):	-	-	-	-	-	-	-	-	-	-	-	-	-	-	-	-	-	-	-	-	-	-	-	-
INV-3	**PV P(W):**	1070	3607	5751	2739	2773	2688	2811	2776	2870	3114	1949	451	3	0	0	0	0	0	0	0	0	0	26	409
	Load P(W):	2804	2741	2701	2648	2606	2709	2690	2618	2668	2708	2725	2814	2776	2607	2677	2626	2446	2824	2487	2453	2473	2686	2655	2530
	EDG P(W):	-	-	-	-	-	-	-	-	-	-	-	-	-	-	-	-	-	-	-	-	-	-	-	-
INV-4	**PV P(W):**	1220	3754	5894	2500	2583	2555	2618	2610	2589	2113	1720	361	32	0	0	0	0	0	0	0	0	0	318	516
	Load P(W):	2783	2778	2765	2546	2544	2570	2634	2579	2579	2735	2814	2806	2720	2666	2699	2603	2754	2448	2345	2186	2691	2724	2290	2449
	EDG P(W):	-	-	-	-	-	-	-	-	-	-	-	-	-	-	-	-	-	-	-	-	-	-	-	-
B-1	**S.O.C (%):**	87.37	89.01	93.63	100	100	100	100	100	100	100	100	98.25	83.56	76.1	69.88	64.6	61.94	61.9	61.4	59.1	48.2	40.24	30.2	28.5
B-2	**S.O.C (%):**	87.47	88.51	93.47	100	100	100	100	100	100	100	100	98.24	85.9	79.72	73.44	68.2	65.31	64.39	60.4	60.1	52.9	45.88	36.6	34.6
B-3	**S.O.C (%):**	89.03	90.84	94.39	100	100	100	100	100	100	100	100	98.79	87.89	82	76.43	70.1	66.65	66.33	65.1	59.1	54.5	48.25	39.4	37.6
B-4	**S.O.C (%):**	88.46	90.39	93.88	100	100	100	100	100	100	100	100	99	89.61	81.32	75.66	69.4	66.8	67.64	64.6	60.7	53.6	47.43	37.6	36.8
B-5	**S.O.C (%):**	89.25	91.8	94.25	99.99	99.99	99.99	100	99.99	99.99	100	100	94.23	85.81	83.44	78.42	72.1	68.57	69.37	65.7	61.8	55.7	50.22	50.2	40.4
B-6	**S.O.C (%):**	89.14	91.8	94.4	100	100	100	100	100	100	100	100	95.12	87.03	84.07	79.3	72.9	69.41	70.57	66.7	60.5	56.7	51.05	50	41.1
B-7	**S.O.C (%):**	89.02	91.21	94.65	100	100	100	100	100	100	100	100	94.35	84.22	82.46	77.4	70.9	67.34	69.03	64.8	59.5	54.3	48.27	48.3	37.7
B-8	**S.O.C (%):**	88.35	90.58	94.94	100	100	100	100	100	100	100	100	93.8	82.9	76.78	76.01	75.9	64.94	68.88	63.3	57.9	52	41.79	41.7	34.3
B-9	**S.O.C (%):**	87.86	90.38	95.44	100	100	100	100	100	100	100	92.18	92.18	84.96	79.52	73.34	66.5	62.86	67.18	61.8	55.9	49.2	45.3	45.3	30.5
B-10	**S.O.C (%):**	87.7	90.2	95.06	100	100	100	100	100	100	100	92.52	90.52	84.19	78.54	70.57	67.7	64.03	63.37	62.5	57	50.8	43.6	42.5	32.2
B-11	**S.O.C (%):**	88.04	88.69	95.19	100	100	100	100	100	100	100	93.1	91.12	85.55	80.34	70.56	69.1	65.45	67.81	63.5	58.5	53	46.04	45.5	35.6
B-12	**S.O.C (%):**	87.78	88.89	9498	100	100	100	100	100	100	100	90.16	91.1	85.21	79.9	73.87	68.3	64.57	67	62.6	57.4	51.8	45.04	40.2	33.7
B-13	**S.O.C (%):**	88.44	89.36	94.92	100	100	100	100	100	100	100	91.21	91.23	86.61	82.05	76.45	70.6	66.67	69.5	64.6	59.4	54.1	48.12	40	37.5
B-14	**S.O.C (%):**	89.28	91.4	96.24	100	100	100	100	100	100	100	91.1	91.1	86.59	81.7	76.01	70.4	69.17	69.7	64	59.2	54	44.59	44.6	37
B-15	**S.O.C (%):**	88.28	90.73	96.2	100	100	100	100	100	100	100	89.86	89.85	84.81	79.78	73.3	68.1	64.2	68.31	62.2	57	51.2	47.69	47.5	23.2
B-16	**S.O.C (%):**	88.23	90.71	95.99	100	100	100	100	100	100	100	87.95	86.95	82.44	76.78	70.44	68.4	62.25	66.93	60.6	55.1	48.8	41.69	41.5	30.6

References

1. Shaqsi, A.Z.; Sopian, K.; Al-Hinai, A. Review of energy storage services, applications, limitations, and benefits. *Energy Rep.* **2020**, *6*, 288–306. [CrossRef]
2. Opeyemi, B.M. Path to sustainable energy consumption: The possibility of substituting renewable energy for non-renewable energy. *Energy* **2021**, *228*, 120519. [CrossRef]
3. Solaun, K.; Cerdá, E. Climate change impacts on renewable energy generation. A review of quantitative projections. *Renew. Sustain. Energy Rev.* **2019**, *116*, 109415. [CrossRef]
4. Halkos, G.E.; Gkampoura, E.C. Reviewing usage, potentials, and limitations of renewable energy sources. *Energies* **2020**, *13*, 2906. [CrossRef]
5. Basit, M.A.; Dilshad, S.; Badar, R.; Sami ur Rehman, S.M. Limitations, challenges, and solution approaches in grid-connected renewable energy systems. *Int. J. Energy Res.* **2020**, *44*, 4132–4162. [CrossRef]
6. Moriarty, P.; Honnery, D. The limits of renewable energy. In *Switching Off: Meeting Our Energy Needs in a Constrained Future*; Springer: Singapore, 2022; pp. 35–54.
7. Ahmed, A.; Ge, T.; Peng, J.; Yan, W.C.; Tee, B.T.; You, S. Assessment of the renewable energy generation towards net-zero energy buildings: A review. *Energy Build.* **2022**, *256*, 111755. [CrossRef]
8. Fatima, N.; Li, Y.; Ahmad, M.; Jabeen, G.; Li, X. Factors influencing renewable energy generation development: A way to environmental sustainability. *Environ. Sci. Pollut. Res.* **2021**, *28*, 51714–51732. [CrossRef]
9. Bhatti, M.Z.; Siddique, A.; Aslam, W.; Atiq, S.; Khan, H.S. Improved model predictive direct power control for parallel distributed generation in grid-tied microgrids. *Energies* **2023**, *16*, 1441. [CrossRef]
10. Khan, H.S.; Aamir, M.; Ali, M.; Waqar, A.; Ali, S.U.; Imtiaz, J. Finite control set model predictive control for parallel connected online ups system under unbalanced and nonlinear loads. *Energies* **2019**, *12*, 581. [CrossRef]
11. Khan, H.S.; Aamir, M.; Kauhaniemi, K.; Mumtaz, M.; Hassan, M.W.; Ali, M. Improved finite control set model predictive control for distributed energy resource in islanded microgrid with fault-tolerance capability. *Eng. Sci. Technol. Int. J.* **2021**, *24*, 694–705. [CrossRef]
12. Abbasi, M.; Abbasi, E.; Li, L.; Aguilera, R.P.; Lu, D.; Wang, F. Review on the microgrid concept, structures, components, communication systems, and control methods. *Energies* **2023**, *16*, 484. [CrossRef]
13. Khalil, L.; Bhatti, K.L.; Awan, M.A.; Riaz, M.; Khalil, K.; Alwaz, N. Optimization and designing of hybrid power system using HOMER pro. *Mater. Today Proc.* **2021**, *47*, S110–S115. [CrossRef]
14. Çetinbaş, İ.; Tamyurek, B.Ü.; Demirtaş, M. Design, analysis and optimization of a hybrid microgrid system using HOMER software: Eskisehir osmangazi university example. *Int. J. Renew. Energy Dev.* **2019**, *8*, 65–79. [CrossRef]
15. Oulis Rousis, A.; Tzelepis, D.; Konstantelos, I.; Booth, C.; Strbac, G. Design of a hybrid AC/DC microgrid using Homer Pro: Case study on an islanded residential application. *Inventions* **2018**, *3*, 55. [CrossRef]
16. Ur Rashid, M.; Ullah, I.; Mehran, M.; Baharom, M.N.; Khan, F. Techno-economic analysis of grid-connected hybrid renewable energy system for remote areas electrification using homer pro. *J. Electr. Eng. Technol.* **2022**, *17*, 981–997. [CrossRef]
17. Raji, A.K.; Luta, D.N. Modeling and optimization of a community microgrid components. *Energy Procedia* **2019**, *156*, 406–411. [CrossRef]
18. Nsengimana, C.; Han, X.T.; Li, L.L. Comparative analysis of reliable, feasible, and low-cost photovoltaic microgrid for a residential load in Rwanda. *Int. J. Photoenergy* **2020**, *2020*, 1–4. [CrossRef]
19. Faiz, F.U.; Shakoor, R.; Raheem, A.; Umer, F.; Rasheed, N.; Farhan, M. Modeling and analysis of 3 MW solar photovoltaic plant using PVSyst at Islamia University of Bahawalpur, Pakistan. *Int. J. Photoenergy* **2021**, *2021*, 6673448. [CrossRef]
20. Kumar, R.; Rajoria, C.S.; Sharma, A.; Suhag, S. Design and simulation of standalone solar PV system using PVsyst Software: A case study. *Mater. Today Proc.* **2021**, *46*, 5322–5328. [CrossRef]
21. Alnoosani, A.; Oreijah, M.; Alhazmi, M.; Samkari, Y.; Faqeha, H. Design of 100mw solar pv on-grid connected power plant using (pvsyst) in umm al-qura university. *Int. J. Sci. Res.* **2019**, *8*, 356–363.
22. Baqir, M.; Channi, H.K. Analysis and design of solar PV system using Pvsyst software. *Mater. Today Proc.* **2022**, *48*, 1332–1338. [CrossRef]
23. Belmahdi, B.; El Bouardi, A. Solar potential assessment using PVsyst software in the northern zone of Morocco. *Procedia Manuf.* **2020**, *46*, 738–745. [CrossRef]
24. Chennaif, M.; Maaouane, M.; Zahboune, H.; Elhafyani, M.; Zouggar, S. Tri-objective techno-economic sizing optimization of Off-grid and On-grid renewable energy systems using Electric system Cascade Extended analysis and system Advisor Model. *Appl. Energy* **2022**, *305*, 117844. [CrossRef]
25. Da Silva, G.D. Utilisation of the System Advisor Model to estimate electricity generation by grid-connected photovoltaic projects in all regions of Brazil. *Int. J. Softw. Eng. Appl.* **2017**, *11*, 1–2. [CrossRef]
26. Karimi, M.; Farshad, M.; Hong, Q.; Laaksonen, H.; Kauhaniemi, K. An Islanding Detection Technique for Inverter-Based Distributed Generation in Microgrids. *Energies* **2021**, *14*, 130. [CrossRef]
27. Kumar, J.; Parthasarathy, C.; Västi, M.; Laaksonen, H.; Shafie-Khah, M.; Kauhaniemi, K. Sizing and Allocation of Battery Energy Storage Systems in Åland Islands for Large-Scale Integration of Renewables and Electric Ferry Charging Stations. *Energies* **2020**, *13*, 317. [CrossRef]
28. Debdouche, N.; Deffaf, B.; Benbouhenni, H.; Laid, Z.; Mosaad, M.I. Direct Power Control for Three-Level Multifunctional Voltage Source Inverter of PV Systems Using a Simplified Super-Twisting Algorithm. *Energies* **2023**, *16*, 4103. [CrossRef]
29. Kumar, J.; Parhyar, N.R.; Panjwani, M.K.; Khan, D. Design and performance analysis of PV grid-tied system with energy storage system. *Int. J. Electr. Comput. Eng.* **2021**, *11*, 1077. [CrossRef]

30. Gul, E.; Baldinelli, G.; Bartocci, P.; Bianchi, F.; Piergiovanni, D.; Cotana, F.; Wang, J. A techno-economic analysis of a solar PV and DC battery storage system for a community energy sharing. *Energy* **2022**, *244*, 123191. [CrossRef]
31. *IEC 61724-1*; Photovoltaic System Performance—Part 1: Monitoring; Edition 2.0. IEC: Geneva, Switzerland, 2021.
32. *IEC TS 61724-2*; Photovoltaic System Performance—Part 2: Capacity Evaluation Method; Edition 1.0. IEC: Geneva, Switzerland, 2016.
33. *IEC TS 61724-3*; Photovoltaic System Performance—Part 3: Energy Evaluation Method; Edition 1.0. IEC: Geneva, Switzerland, 2016.